High Field Magnetic Resonance Facility

The High Field Magnetic Resonance Facility focuses on developing a fundamental, molecular-level understanding of biochemical and biological systems and their response to environmental effects. A secondary focus is in aspects of materials science and catalysis and the chemical mechanisms and processes operative in these areas. Resident and matrixed research staff within this facility offer expertise in the areas of structural biology, solid-state materials/catalyst characterization, magnetic resonance imaging (MRI) techniques, and high-resolution spectroscopy of biological objects using a slow (1-100 Hz) magic angle spinning.

Research activities include structure determination of large molecular assemblies such as protein, DNA (normal and damaged), and RNA complexes as a cellular response to chemical or radiological insults; conformational changes in membrane protein complexes involving metal clusters as followed by pulsed EPR; NMR-based structural and functional genomics; materials and catalyst characterization via solid-state techniques; non-invasive biological imaging, integrated magnetic resonance and confocal microscopy and slow spinning NMR to study cell systems.

The former Macromolecular Structure & Dynamics directorate operated one of the EMSL's high-volume experimental user facilities–the High Field Magnetic Resonance Facility in support of these and other user research programs from October 1997 through October 2002. Over 130 external scientists and users have been afforded access to the NMR/EPR instruments between October 2001 and December 2002 with an additional 18 scientists gaining access in the second quarter of FY 2003.

Instrumentation & Capabilities

NMR

- 900-MHz NMR (installation in progress)
- 800-MHz NMR
- 750-MHz NMR
- 600-MHz NMR (2 systems)
- 500-MHz WB NMR (2 systems, 1 delivered May '02 – now operational for MRI)
- 500-MHz NMR (2 systems)
- 400-MHz WB NMR
- 300-MHz WB NMR (2 systems)

EPR

- EPR Spectrometer with ENDOR/ELDOR capability

Additional Capabilities

- Combined optical and magnetic resonance microscope
- Low temperature probes for metallo-protein chemistry and structure
- Virtual NMR capability enables use and collaboration with EMSL scientists for remote users via secure shell over the internet

The research interests of the scientific staff include some of the most exciting areas in modern molecular biology and biochemistry.

- Structural Genomics: Determination of three dimensional structures of DNA, RNA, proteins and enzymes, and their bonding and intermolecular associations. Particular interests and collaborations exist relative to protein fold classification and sequence-structure-fold relationships.
- Functional Genomics: Determination of the bonding and interaction domains among DNA, RNA, and proteins, with particular emphasis on DNA damage recognition and repair processes.

- Biological Imaging: Acquisition of imaging and corresponding chemical information in biological samples, with particular interest in development of combined magnetic resonance and optical spectroscopy techniques to observe and elucidate biological processes and slow magic angle spinning methodologies in cells, tissues, small animals and bacterial colonies.
- Measurement Science and Instrumentation Development: Development and application of novel and unique nuclear magnetic resonance (NMR) instrumentation techniques for biological and environmental problems.

Magnetic Resonance Research Capabilities

Varian INOVA 800. The Varian 800 is an INOVA-based spectrometer and an Oxford 18.8-T magnet with a 63-mm room temperature bore. This system is capable of high-resolution-liquid and solid-state NMR. There are four RF channels with waveform generators and pulsed-field gradients. The wideline ADCs run at 5 MHz and the narrow ADCs have a maximum rate of 500 kHz. Available probes include two 5-mm HCN probes with Z gradient for liquids, 4-mm HXY MAS probe (25-kHz spinning), a 7.5-mm orthogonal powder probe and a 5-mm HX orthogonal powder probe optimized for low gamma nuclides. Under construction are a 5-mm HX MAS probe (12 kHz spinning), and a 5-mm HX static low temperature probe (3.8-300K).

Varian INOVA 750. The Varian 750 is an INOVA-based spectrometer and an Oxford 17.6-T magnet with a 51-mm room temperature bore. This system is capable of high-resolution-liquid, solid-state NMR. There are four RF channels with waveform generators and pulsed field gradients. The narrow ADCs have a maximum rate of 500 kHz. We currently have two 5-mm HCN probes (Z gradient), a 5-mm HCP probe (Z gradient), and a 5-mm HX MAS probe (X tuning range is 321–130 MHz; the spinning speed is rated to 12 KHz). Under construction are two 5-mm HX MAS probes (15 kHz spinning) with X tuning ranges of 130–60 MHz and 60–25 MHz.

Varian INOVA 600. The Varian 600 is an INOVA-based spectrometer and an Oxford 14.1-T magnet with a 51-mm room temperature bore. This system is capable of high-resolution-liquid NMR. There are four RF channels with waveform generators and pulsed-field gradients. The narrow ADCs have a maximum rate of 500 kHz. We currently have a 5-mm HCN probe with Z gradient and a 5-mm HX probe (X tuning range 242–60 MHz).

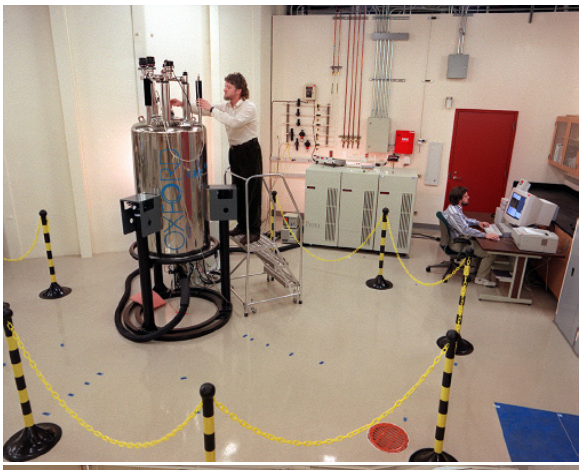

Varian Unity 600. Varian 600 is a Unity-based spectrometer and an Oxford 14.1-T magnet with a 51-mm room temperature bore. This system is capable of high-resolution-liquid NMR. There are three RF channels with waveform generators and pulsed-field gradients. The narrow ADCs have a maximum rate of 500 kHz. We currently have a 5-mm HCN probe with Z gradient and a 5-mm HX probe (X tuning range 242–60 MHz).

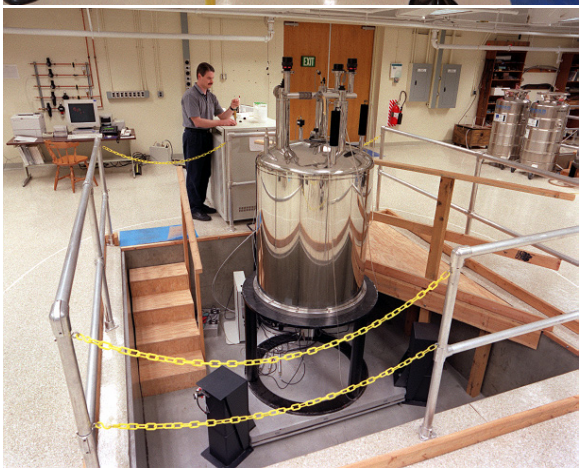

Varian Unity+ 500 WB. The Varian 500 WB is a Unity-based spectrometer and an Oxford 11.7-T magnet with an 89-mm room temperature bore. This system is capable of solid-state NMR, μ-imaging, and small animal MRI. There are three RF channels with waveform generators. The wideline ADCs run at 5 MHz. We currently have a 5-mm orthogonal powder probe, 5-mm HXY MAS probe (15 kHz spinning), a 7-mm HX MAS probe (10 kHz spinning), an HX single crystal probe, a 1H CRAMPS probe, a micro-coil imaging probe, and a 40-mm imaging probe. Under construction is a static HX low temperature probe (2–300 K).

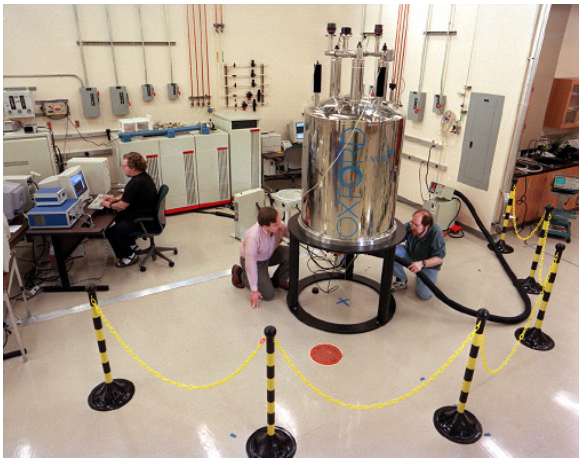

Bruker Avance 500 WB. The Bruker Avance 500 is a micro-imaging system using an 89-mm vertical room temperature bore. The system is capable of imaging mice, and also has high-resolution liquid MR capabilities with a Bruker 10-mm QNP probe. This liquids probe has a 1H outer coil and an inner coil that is switchable among 13C, 31P and 19F with no gradients. Finally, the system is equipped with a home-built combined confocal and magnetic resonance microscope, capable of monitoring single layers of eukaryotic cells in a perfusion system simultaneously with both modalities.

Varian/Chemagnetics Infinity 500. The Chemagnetics 500 is an Infinity-based spectrometer and an Oxford 11.7-T magnet with a 51-mm room temperature bore. This system is capable of high-resolution-liquid and solid-state NMR. It has three RF channels and is equipped with both 16 and 14 bit ADCs. The solution state probes for this instrument are a 5-mm HCN gradient probe, a 5-mm DB gradient probe (X tuning range is 208.1 MHz–49.5 MHz), and a 10-mm HX probe (X tuning range is 218.6 MHz–21.2 MHz). The solid-state probe is a 5-mm HX MAS probe (X tuning range is 206.6 MHz–47 MHz; the spinning speed is rated to 12 KHz).

Varian Unity+ 500 NB. The Varian 500 is a Unity-based spectrometer and an Oxford 11.7-T magnet with a 51-mm room temperature bore. This system is capable of high-resolution liquids NMR. There are three RF channels with waveform generators and pulsed-field gradients. We currently have a 5-mm HCN probe with Z gradient and a 10-mm HX probe.

Varian/Chemagnetics Infinityplus 400. The Varian 400 spectrometer is an Infinity+ based spectrometer and an Oxford 9.4-T magnet with a 89-mm room temperature bore. This system is only used for solid-state NMR. There are 2 RF channels and 5-MHz ADCs. We currently have a 5-mm HX MAS probe, a 5-mm HX static cryogenic probe (3.8–300 K), a 7-mm HX static low temperature probe (4.2-400 K), a 10-mm HX DAS probe, and all of the Unity+ 500 WB broadband probes may be used in single channel mode.

Varian/Chemagnetics Infinity 300. The Chemagnetics 300 is an Infinity-based spectrometer and an Oxford 7.02-T magnet with a 89-mm room temperature bore. This system is capable of high-resolution-liquid and solid-state NMR. It has three RF channels and is equipped with both 16 and 14 bit ADCs. The solution-state probes for this instrument are a 5-mm HX probe and a 10-mm HX probe. The solids probes are a 7.5-mm HX MAS probe (X tuning range is 136.7 MHz–29.5 MHz; H tuning range is 274.7 MHz–349.1 MHz; spin rate is rated to 7 Hz) and a 5-mm HXY MAS probe (X tuning range is 129 MHz–57.4 MHz; Y-tuning range is 85.1 MHz–21.2 MHz; spin rate is rated to 12 KHz).

Varian Unity+ 300. The Varian 300 is a Unity-based spectrometer and an Oxford 7.04-T magnet with an 89-mm room temperature bore. This system is capable of solid-state NMR, μ-imaging, and small animal MRI. There are two RF channels with wideline ADCs running at 5 MHz. We currently have a 7-mm HX MAS probe (10-kHz spinning), an HX single crystal probe, a 1H CRAMPS probe, a single-tuned DOR probe, an HX 5-mm, low-temperature MAS probe (35–300K, 12-kHz

spinning), a 7-mm HX high temperature probe (-100 to 500°C, 7 kHz spinning), a microscopy probe, and a 40-mm imaging probe.

Bruker Pulsed EPR/ENDOR/ELDOR Spectrometer. The EPR/ENDOR work focuses on the development and application of pulsed, two-dimensional methods for electronic structure and distance determinations in biological macromolecules and materials. The spectrometer consists of a Bruker 380E Pulsed EPR Spectrometer with pulsed ENDOR and has been modified to include pulsed ELDOR capabilities.

900 MHz NMR Magnet Upgrade

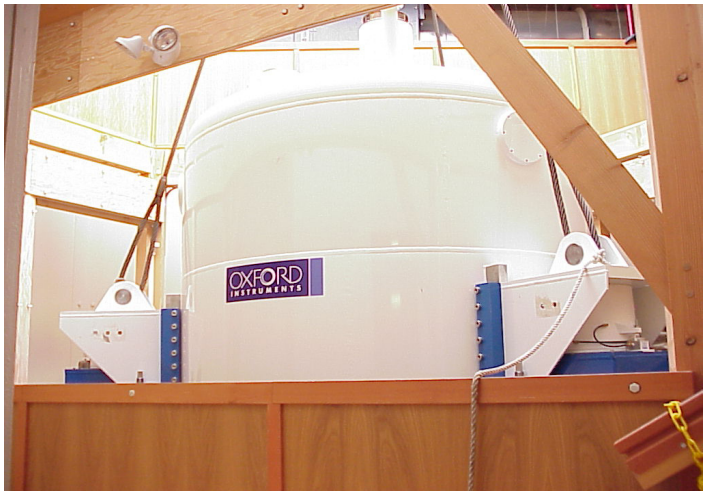

EMSL's long-awaited 900 MHz, wide-bore NMR magnet was delivered in March 2002 after nearly 10 years of development effort. The magnet was designed and manufactured by Oxford Instruments (Oxford, UK). The magnet, comprising 200+ miles of specialty-formulation, superconducting wire, and weighing over 16 tons, operates at a field of 21 T with 27 MJ of stored energy. Magnet installation, commissioning, stabilization, and testing activities have been conducted. The 900 MHz NMR capability will be made available to users toward the end of FY 2003, enabling enhanced structural studies of biological and environmental molecules and systems.

Combined Magnetic Resonance and Optical Microscope

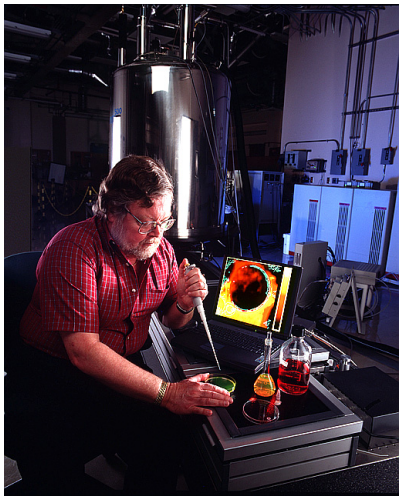

Housed at the EMSL NMR User Laboratory at PNNL, it uses an 89-mm diameter, vertical-bore, 11.7-T Oxford magnet (WB500), into which a bottom-loading OM probe and a top-loading MRM probe are inserted. The sample compartment contains an optical window and a solenoid NMR coil wound onto a horizontally aligned, 0.82-mm ID silica capillary sample tube. The sample tube is part of a perfusion system used to transport the cells to the test section and to maintain cell viability. (The confocal beam enters the sample transverse to the coil and is partially attenuated by the coil turns; therefore, the coil design is a compromise between NMR sensitivity and correctable optical distortion.)

Cryogenic NMR Probe Development

The critical role metals play in biology requires a detailed understanding of the chemistry, structure, and bonding within the complexes and how, in turn, these manifestations alter the chemistry at the metal binding site. The potential chemistry that occurs at the metal binding site is reflected in the magnetic resonance parameters, which are sensitive to charge, ligand type and number, and the symmetry of the site. A methodology has been developed here at the EMSL to facilitate the direct observation of these metals (e.g., ^{67}Zn and ^{25}Mg) in dilute environments such as in a metalloprotein. This method involves use of a cryogenic NMR probe that routinely operates at 10 K. Currently in operation are 5-mm static, double resonance probes at 9.4 and 11.7 T with a similar probe being developed at 18.8 T and triple resonance capabilities in the design phase.

Supercritical Fluids Accessory

A potential limitation to liquid-state NMR experiments occurs when the rotational correlation time of the molecule of interest becomes so long that significant line broadening occurs which in turn limits resolution and sensitivity. Hence, it is of interest to develop solvent systems that can extend the limits of rotational correlation times. Supercritical solvents represent such a system. These solvents also have the advantage that they process novel solvent chemistry and catalytic properties. To support DOE sponsored activities, we have developed a system to allow characterization of solutes by NMR and EPR under supercritical conditions. This capability is being applied to develop an understanding of the field dependence of dynamic nuclear polarization experiments as they relate to signal enhancement methods for characterization of homogeneous and heterogeneous catalysts. The EMSL system is based on fused silica capillaries and employs two pumps. The first pump is a low-pressure pump (ISCO) capable of 10,000 psi (~0.67 kbar) and an operating volume of 100 mL. The second pump is a high-pressure pump (High Pressure Equipment Corporation) capable of 60,000 psi (~4 kbar) and an operating volume of 10 mL.

An NMR Approach to Structural Proteomics

CH Arrowsmith,[(a)] AA Yee,[(a)] X Change,[(a)] A Pineda-Lucena,[(a)] J Liao,[(a)] B Wu,[(a)] A Semesi,[(a)] B Le,[(a)] AM Edwards,[(b)] MA Kennedy,[(c)] JR Cort,[(c)] and TA Ramelot[(c)]

(a) University of Toronto, Ontario, Canada
(b) Ontario Cancer Institute, Toronto, Canada
(c) Pacific Northwest National Laboratory

This project is a collaboration with Michael Kennedy at EMSL and is funded by both structural genomics grants (NIH and Canadian granting agencies) as well as traditional hypothesis driven research grants from Canadian sources. For both types of research we are also very interested in developing methods and strategies that will make protein structure determination by NMR faster and more efficient. Highlights from the past 2 years of our research that have made use of EMSL NMR spectrometers are discussed below; details are reported in the articles listed in the References.

We wish to understand protein biochemical function through the use of NMR spectroscopy and the derivation of solution structures from NMR data. The rationale for such an approach is that protein three-dimensional structure is a fundamental unit of genomic information, and a complete functional map of the proteome must ultimately consist of the three-dimensional structures for all proteins. In the post genomic era, NMR can help to achieve such a goal by 1) providing fundamental insights into the mechanism of action of proteins of known function, 2) suggesting functional roles for novel proteins of unknown function, and 3) providing an experimental tool for the interpretation of functional data such as mutagenesis, protein-protein interaction studies and ligand binding analysis.

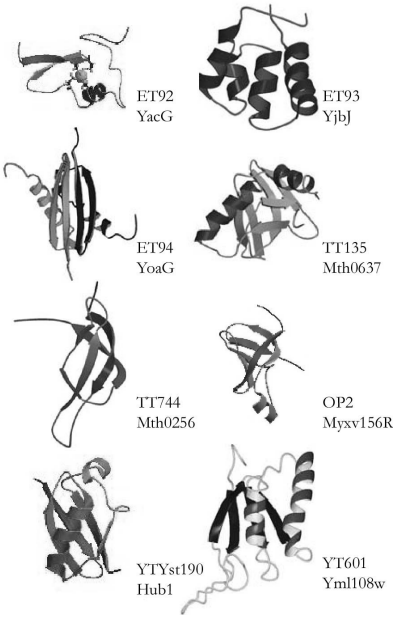

Figure 1. Molscript ribbon representations of 8 structures determined by NMR spectroscopy. ET proteins are from *Eschericia coli*, TT from *Methanobacterium thermoautotriphicum*, YT from *Saccharomyces cerevisiae*, and OP from *myxoma* virus. PDB ids are 1LV3, 1JYG, 1NE1, 1JRM, 1NE3, 1JJG, 1M94, and 1N6Z.

As reported in Yee et al. (2002), we surveyed over 500 small proteins from several organisms and found ~20 % of these proteins were found to be readily amenable to NMR structure determination. NMR sample preparation was centralized in one facility, and a distributive approach was used for NMR data collection and analysis. EMSL played a central role in our data collection strategy. Twelve new structures are reported in this paper that allowed us to infer putative functions for several conserved hypothetical proteins (several shown in Figure 1). This paper was very popular, receiving one of the highest number of "hits" on the PNAS website for the month it was published.

Here we report five protein structures which were solved in our laboratory and four which were solved by collaboration with Michael Kennedy. NMR data for all proteins were

acquired at EMSL. In all cases, the target proteins were chosen because they didn't have sequence similarity to any proteins of known structure below the cut-off of 10^{-4} as determined by a BLAST search of the PDB database. Most of the proteins chosen were conserved hypothetical proteins with no functional annotation. In several cases, possible biochemical functions could be inferred from the 3-D structures. ET94 is a homodimer and ET92 is a zinc finger, however the functions remain unknown. YT601 may have an RNA-binding motif. TT744 and OP2 have a common nucleic acid binding fold. TT744 has high homology to ribosomal protein S28E and may be involved in control of translational accuracy. Structural similarity between OP2 and the N-terminal domain of eukaryotic eIF2α suggested that it would be a PKR (interferon-induced protein kinase) substrate, which was then demonstrated. YTYst190 has the ubiquitin-like fold and has been shown to be a ubiquitin-like modifier protein involved in yeast cell polarization. TT135 and YT601 have no known biological function, but the 3-D structures reveal novel variations of two α/β fold superfamilies. ET93 is a four helix bundle protein with no sequence homologs. Many of these proteins provide a novel link between sequence and 3-D structures. These structures extend our knowledge of protein structure space and will help modelers in the future in protein modeling and structure prediction.

References

Kennedy, MA, GT Montelione, CH Arrowsmith, and JL Markley. Role for NMR in structural genomics. *Journal of Structural and Functional Genomics*, **2**, 155-169 (2002).

Pineda-Lucena, A, GS Yi, X Chang, JR Cort, MA Kennedy, AM Edwards, and CH Arrowsmith. Solution structure of the hypothetical protein MTH0637 from *Methanobacterium thermoautotrophicum. Journal of Biomolecular NMR*, **22**, 291-294 (2002).

Pineda-Lucena, A, J Liao, A Yee, JR Cort, MA Kennedy, AM Edwards, and CH Arrowsmith. NMR structure of the hypothetical protein encoded by the YjbJ gene from *Eschericia coli. Proteins: Structure, Function, and Genetics*, **47**, 572-574 (2002).

Ramelot, TA, JR Cort, AA Yee, A Semesi, AM Edwards, CH Arrowsmith, and MA Kennedy. NMR Structure of the *Eschericia coli* protein YacG: A novel sequence motif in the zinc-finger family of proteins. *Proteins: Structure, Function, and Genetics*, **49**, 289-293 (2002).

Ramelot, TA, JR Cort, AA Yee, A Semesi, AM Edwards, CH Arrowsmith, and MA Kennedy. Solution structure of yeast ubiquitin-like modifier protein Hub1. *J. Structural and Functional Genomics*, in press.

Ramelot, TA, JR Cort, AA Yee, F Liu, MB Goshe, AM Edwards, RD Smith, CH Arrowsmith, TE Dever, and MA Kennedy. Myxoma virus immunomodulatory protein M156R is a structural mimic of eukaryotic translation initiation factor eIF2α. *Journal of Molecular Biology*, **322**, 943-954 (2002).

Yee, A, X Chang, A Pineda-Lucena, B Wu, A Semesi, B Le, T Ramelot, GM Lee, S Bhattacharyya, P Gutierrez, A Denisov, C-H Lee, JR Cort, K Guennadi, J Liao, G Finak, L Chen, D Wishart, W Lee, LP McIntosh, K Gehring, MA Kennedy, AM Edwards, and CH Arrowsmith. An NMR approach to structural proteomics. *Proceedings of the National Academy of Science, USA*, **99**, 1825-1830 (2002).

Molecular Structure of BAG Proteins

K Briknarová,[(a)] S Takayama,[(a)] L Brive,[(a)] S Homma,[(a)] ML Havert,[(a)] K Baker,[(a)] DA Knee,[(a)] J Velasco,[(a)] J Stuart,[(a)] Z Li,[(a)] E Cabezas,[(a)] DW Hoyt,[(c)] AC Satterthwait,[(a)] MA Llinás,[(b)] JC Reed,[(a)] and KR Ely[(a)]

(a) The Burnham Institute, La Jolla, California
(b) Carnegie Mellon University, Pittsburgh, Pennsylvania
(c) W.R. Wiley Environmental Molecular Sciences Laboratory

BAG proteins are conserved throughout eukaryotes, with homologues found in vertebrates, insects, nematodes, yeast, and plants. The human members of this family include BAG1, BAG2, BAG3 (CAIR-1/Bis), BAG4/SODD (Silencer of Death Domains), BAG5, and BAG6 (BAT3/Scythe). BAG proteins contain diverse N-terminal sequences but share a conserved protein interaction module near the C-terminal end called the BAG domain (BD). The BD binds to the ATPase domain of Hsp70/Hsc70 and modulates activity of these molecular chaperones. The BD of BAG1 also interacts with the C-terminal catalytic domain of Raf-1 and activates the kinase. It has been proposed that BAG family members serve as "toggles" in cell signaling pathways. For example, Raf-1 and Hsp70 may compete for binding to BAG1.

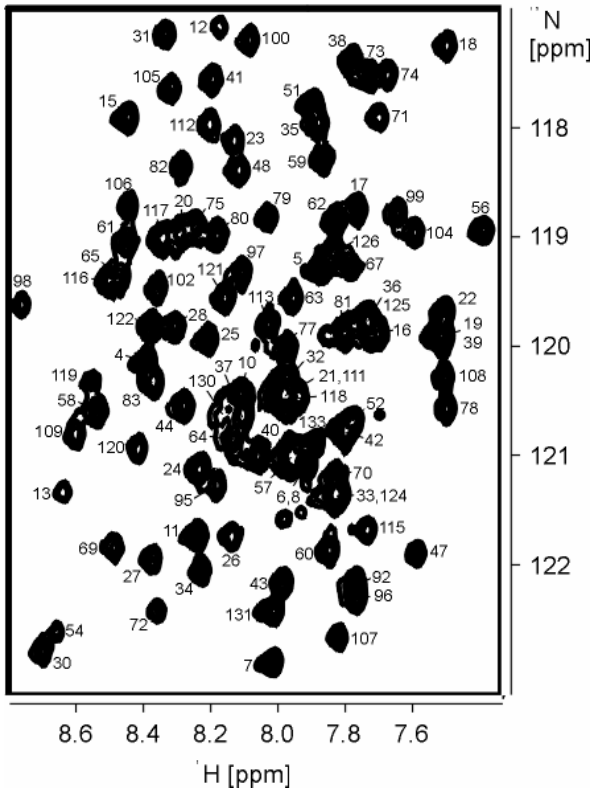

Figure 1. Central region of ^{1}H-^{15}N HSQC spectrum of the BAG domain from BAG1. Resonance assignments are indicated.

When levels of Hsp70 are elevated after cell stress, the BAG1/Raf-1 complex is replaced by BAG1/Hsp70, and DNA synthesis is inhibited. Thus, BAG1 serves as molecular switch between cell proliferation and growth arrest. BAG4 (SODD), on the other hand, may play a role as a cellular "adaptor." It has been speculated that BAG4 recruits Hsc70 to tumor necrosis factor receptor 1 (TNFR1) and death receptor 3 (DR3), inducing conformational changes that prevent receptor signaling in the absence of ligand.

Each of the human BAG proteins binds to Hsp70/Hsc70 and modulates their chaperone activity. The conserved BD is necessary and sufficient for this interaction. We have determined the solution structures of the BDs from BAG1 and BAG4, using NMR (Briknarová et al. 2001, 2002). The crosspeaks in ^{1}H-^{15}N HSQC spectra of the BDs from BAG1 and BAG4 (Figures 1 and 2) are rather clustered, which is typical for highly helical

proteins. Hence, data were collected on 600 and 750 MHz spectrometers at EMSL to relieve the spectral overlap and to improve the resolution. Virtually complete ^{1}H, ^{13}C and ^{15}N assignments were established based on several triple resonance experiments, including 3D HNCACB, CBCA(CO)NH, C(CO)NH, H(CCO)NH, HCCH-TOCSY, HNCO and CBCACOHA. 3D ^{15}N-edited NOESY, 3D $^{13}C/^{15}N$-edited NOESY, 4D $^{15}N/^{15}N$-edited NOESY and 4D $^{13}C/^{13}C$-edited NOESY spectra were used to facilitate the assignments and to generate distance restraints.

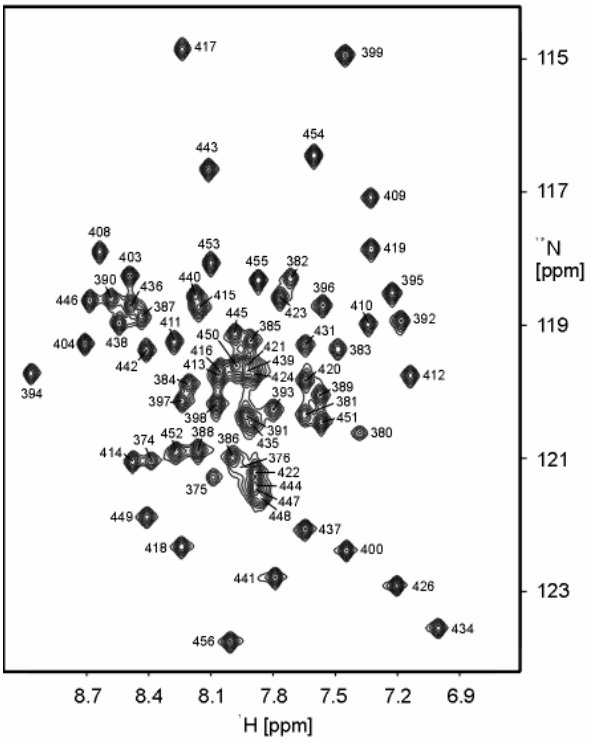

Figure 2. Central region of ^{1}H-^{15}N HSQC spectrum of the BAG domain from BAG4.

Both BDs are three-helix bundles (Figure 3). However, the BD in BAG4 is significantly shorter than its counterpart in BAG1. Our structural studies thus not only identified a novel fold but also revealed two subfamilies of BAG domains that are structurally distinct.

Figure 3. BAG domain is a three-helix bundle. Superimposed backbone traces of a family of 25 structures of the BAG domain from BAG1

References

Briknarová, K, S Takayama, L Brive, ML Havert, DA Knee, J Velasco, S Homma, E Cabezas, J Stuart, DW Hoyt, AC Satterthwait, M Llinás, JC Reed, and KR Ely. Structural analysis of BAG1 cochaperone and its interactions with Hsc70 heat shock protein. *Nature Structural Biology*, **8**, 349-352 (2001).

Briknarová, K, S Takayama, S Homma, K Baker, E Cabezas, DW Hoyt, Z Li, AC Satterthwait, and KR Ely. BAG4/SODD protein contains a short BAG domain. *Journal of Biological Chemistry*, **277**, 31172-31178 (2002).

High Field Solution State ^{27}Al and ^{1}H NMR of Methylaluminoxane

LG Butler,[(a)] JL Eilertsen,[(a)] WD Treleaven,[(b)] and J Ford[(b)]
(a) Louisiana State University, Baton Rouge
(b) W.R. Wiley Environmental Molecular Sciences Laboratory

Methylaluminoxane (MAO) is the most widely used activator for metallocene-based catalysts for olefin polymerization. Despite continuous research since it was accidentally discovered about 25 years ago, its structure and mode of working is not known. The composition of MAO is experimentally determined to $Me_{1.4\text{-}1.5}AlO_{0.8\text{-}0.75}$ with average molecular weight of 1100 Da (Babushkin et al. 1997). From an ^{27}Al resonance around 155 ppm it has been suggested that aluminum is 4-coordinate in MAO, but recently it was pointed out that this resonance probably belongs to trimethylaluminium (TMA) that is always present in MAO solutions (Imhoff et al. 1998). A broad resonance around 110 ppm, still in the region for 4-coordinate aluminum, has been observed at temperatures from about 40ºC and up. This resonance is close to the observed resonance of the *tert*-butylalumoxanes $(tBuAlO)_6$ and $(tBuAlO)_9$, and it was suggested that it is due to $(MeAlO)_n$ formed by splitting off TMA from MAO. IR spectroscopy shows no major change on heating; hence, we expected the growth of the resonance at 110 ppm to be due to faster exchange kinetics rather than changes in the molecular constituents. Our aim was to investigate this signal at higher field than previously applied.

1,4-Dioxane was chosen as the solvent since it was expected to block chemical exchange between MAO and TMA in the mixture. Spectra were recorded at 25 to 70ºC on EMSL's 750 MHz spectrometer (Figure 1). Unfortunately, no resonance at 110 ppm was observed. The quality of the sample was verified by the proton spectrum. A conclusion about why the resonance remained unobservable under these conditions has not been determined. The higher viscosity of 1,4-dioxane compared to toluene may play an important role. In summary, the desired ^{27}Al spectrum of MAO was not acquired, probably due to a large line width (long correlation time and very large quadrupole coupling constants).

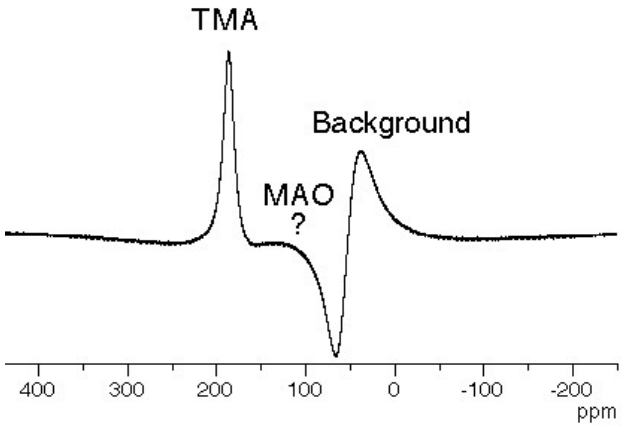

Figure 1. Solution ^{27}Al NMR at 70 °C at 195 MHz (17.6 T, 750 MHz ^{1}H) of MAO in 1,4-dioxane showing TMA and probe background. The TMA resonance represents less than 10% of the Al in the sample.

The proton spectrum of MAO recorded at 750 MHz (Figure 2) shows interesting fine structure that had not been noted at lower field. The proton spectrum of MAO contains a featureless 1 ppm wide resonance, and so far there have been few attempts to verify the reason for this feature. It has mostly been explained by the presence of multiple species involved in equilibrium reactions in the complicated MAO mixture. The observation of a fine structure suggests that it is not due to a few severely broadened resonances, but a greater number of peaks with slow exchange kinetics. Experiments using partial presaturation of the spectrum confirmed this view. Further investigations are planned based on these findings. The solution ^{27}Al NMR spectra in a less viscous/interacting solvent are of great importance.

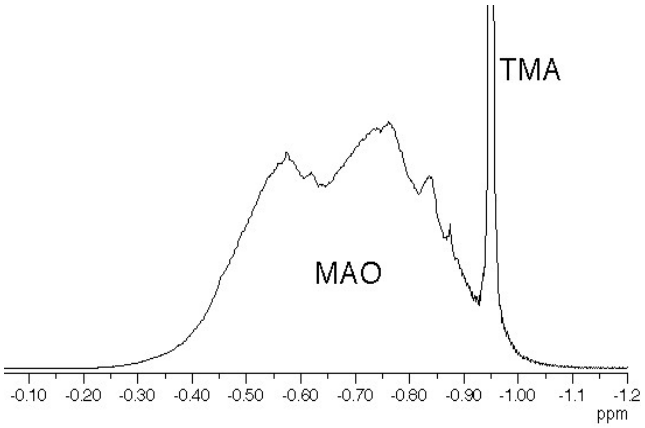

Figure 2. $^{1}H\{^{13}C\}$ spectrum of MAO in 1,4-dioxane at 750 MHz. The sharp signal at –0.95 ppm is due to the TMA-dioxane adduct.

References

Babuskhin, DE, NV Semikolenova, VN Panchenko, AP Sobolev, V Zakharov, and EP Talsi, *Macromol Chem Phys.*, **198**, 3845 (1997).

Imhoff, DW, LS Simeral, SA Sangokoya, and JH Peel. *Organometallics*, **17**, 1941 (1998).

Solid State ^{133}Cs and ^{23}Na NMR of Zeolitic Minerals Found in Sediment Reacted with Simulated Hanford Tank Waste Solutions

Y Deng,[(a)] JJ Ford,[(b)] JB Harsh,[(a)] and M Flury[(a)]
(a) Washington State University, Pullman
(b) W.R. Wiley Environmental Molecular Sciences Laboratory

Several zeolite or zeolite-like minerals have been found in Hanford sediments reacted with solutions simulating the high-level radioactive waste solutions stored in the underground tanks at the DOE Hanford site. The new mineral phases, especially the colloid sized particles, may facilitate the transport of radioactive nuclides in the vadose zone. Cancrinite, sodalite, Linde Type A (LTA) zeolite, and a short-range ordered material, allophane, have been found in our previous simulation experiments. These zeolite-like materials have high negative charge sites in their structures and are capable of incorporating and sorbing cationic radionuclides such as Cs^+ in their framework and on external surfaces. The zeolite-like minerals have unique cages and channels within their structures where the radionuclides might be trapped. The incorporated or sorbed radionuclides may occupy different cages. Because the sizes of the cages are different, some cages may be easier to access than others. For the same reason, the radionuclides may have different stability if they stay in different cages. It also has been observed that OH^-, NO_3^-, CO_3^{2-}, SO_4^{2-}, NO_2^-, and Cl^- anions can be incorporated in cancrinite or sodalite. It is possible that the radionuclides form ion pairs with these anions in the minerals. It is critical to understand the chemical environments of the sorbed and incorporated radionuclides, such as cesium, in the minerals, because the environment determines the association, and the association determines the stability of the radionuclides in the minerals. In this experiment, we used solid state magic angle spin nuclear resonance spectroscopy (MAS NMR) to study the chemical environment of the incorporated and adsorbed ^{133}Cs in the newly formed minerals. We also studied ^{23}Na NMR of the samples before and after cesium incorporation and adsorption. Within a one-week instrument time limitation, we finished the room temperature ^{23}Na NMR and part of the ^{133}Cs NMR analyses.

The radius and valence of the ions, and the size of the cages inside the minerals play important roles in the adsorption and exchange of ions in the zeolitic minerals. Cs^+ cannot easily access the internal cages of cancrinite or sodalite because of its larger ionic radius of 0.167 nm, but it can access LTA zeolite. Incorporated and sorbed Cs^+ showed different ^{133}Cs peak positions (e.g., the Linde Type A zeolite, Figure 1a), indicating different chemical environments. We speculated that the adsorbed cesium cations stay in the larger α cages of LTA zeolite while the incorporated cesium stayed in the smaller β cages. Cesium cannot migrate from one type of cage to the other due to the large size of the cesium cations. For the same reason, incorporated Cs^+ cannot be easily replaced by other ions (e.g., Ca^{2+} or K^+). Although there are two mineral phases, cancrinite and sodalite, formed in the lepispheres synthesized in 1 M NaOH and 0.5 M $NaNO_3$ solution (Figure 1b), and Na^+ can exist as exchangeable cation and ion pairs in the different cages, only one peak showed in most of the ^{23}Na NMR patterns. Incorporating or adsorbing Cs^+ or other cations did not distinctly

shift the peak position or split the peak. This can be the result of the high motion of Na^+ ions and water molecules inside the cages or channels which averaged out the chemical environment of the ions, as has been suggested in other zeolite minerals (e.g., Ahn and Iton, 1991). Although the ionic radius of Ca^{2+} (0.099 nm) is very close to the radius of Na^+ (0.097nm), calcium ions have more difficulty accessing the internal cages of cancrinite or sodalite than the larger K^+ ions. We believe this difference between mono- and di-valent cations is due to restrictions brought about by charge localization in the cages of the minerals. The β or ε cages of cancrinite or sodalite are smaller than the α cages of LTA zeolite and, therefore, the charges from the framework are more localized. The localized high charge density might be better balanced by the monovalent cations on a 1:1 ratio. The source charges are smeared out in larger α cages of LTA zeolite and, therefore, had a less restricted ion valence requirement. We are planning to continue more ^{133}Cs and ^{23}Na NMR studies at low temperature after removing the moisture from the samples. Low temperature will slow down the motion of the ions and will enable us to get a more sound assignment.

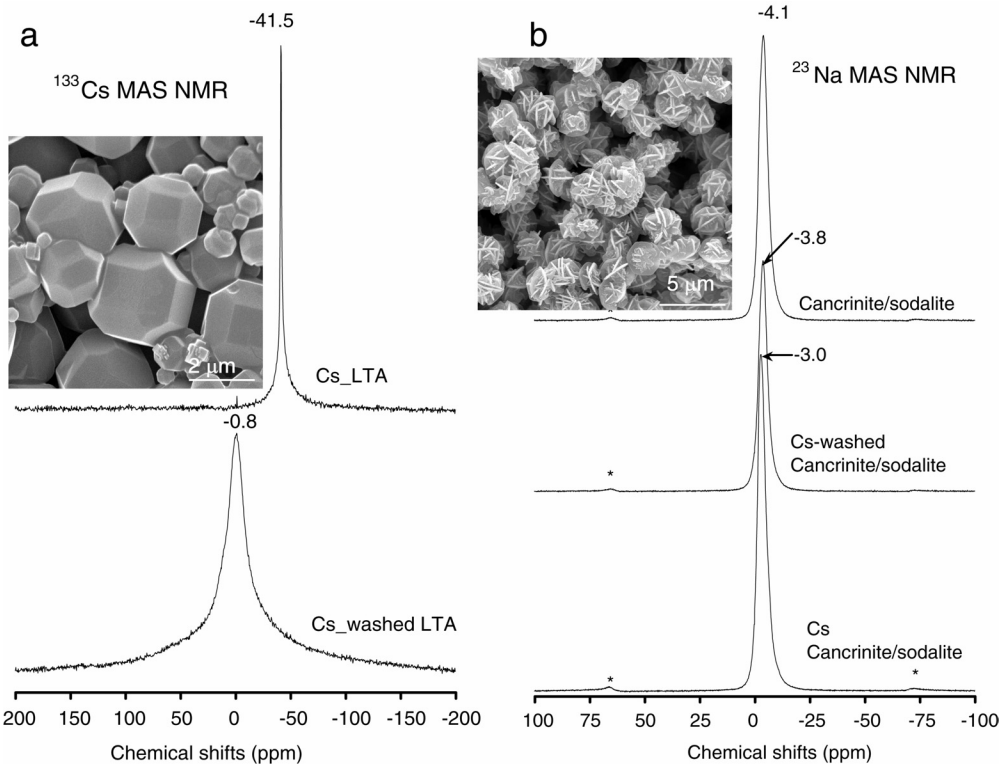

Figure 1. a. Solid state ^{133}Cs MAS NMR of Linde Type A (LTA) zeolite; b. Solid state ^{23}Na MAS NMR of cancrinite/sodalite lepispheres.

Reference

Ahn, MK, and LE Iton. Solid-state cesium-133 NMR studies of cations in cesium/lithium/sodium zeolite A: An example of cation dynamics involving three sites. *J. Phys. Chem.* **95**:4496-500 (1991).

Solid State NMR Structural and Dynamic Studies of Hydrated Salivary Histatin-5 Bound on Hydroxyapatite

M Cotten,[(a)] GP Drobny,[(b)] and PS Stayton[(b)]
(a) Pacific Lutheran University, Tacoma, Washington
(b) University of Washington, Seattle

Biomineralization is a field that studies the formation of mineral tissues by organisms, offering structural biologists many opportunities to address some core issues of structure-function relationships and molecular recognition at interfaces. Some important implications of better understanding biomineralization include new advances in the materials science using biomimetics. To learn more about biomineralization phenomena, we have been studying human salivary polypeptides found in the acquired enamel pellicle. The work presented here focuses on histatin-5, a polypeptide which is histidine-rich, basic, and possesses at least two important functions: control of hydroxyapatite (HAP, calcium phosphate) crystal growth and antimicrobial activity (Brewer and Lajoie 2000; Gusman et al. 2001). Previous studies have characterized functionally important regions of the peptide sequence and some secondary conformation analysis in solution have been done. Very little is known about specific histatin-5/surface interactions and the conformation of the HAP-bound peptide. This knowledge is nevertheless necessary to better understand molecular recognition and structure-function relationships. We have used solid state NMR to characterize the conformation and dynamics of hydrated histatin-5 bound to HAP crystals.

REDOR Experiments on Histatin-5 Samples

At the time of our last report, solid state NMR experiments performed at the University of Washington (UW) and at the EMSL provided some complementary distances measurements that could be used as structural constraints. At the EMSL, we used REDOR (Rotational Echo DOuble Resonance) (Gullion and Schaefer 1989) on the 500 MHz, 89-mm bore, Varian Unity spectrometer fitted with a triple resonant Doty probe. REDOR is a technique that has been successfully and widely used for characterizing $^{13}C/^{15}N$ distances in peptides. Here, the goals were to characterize distances in specifically labeled (i/i+4) $^{13}C/^{15}N$ spin pairs in the backbone of histatin-5.

The XY8 version of REDOR was used since it includes a phase cycling that minimizes experimental imperfections such as off resonance and finite pulse width effects. Two samples were used to set up REDOR: 1) a glycine sample labeled on the carbonyl carbon and amide nitrogen (2.5 Å distance) and 2) α-helical peptide ("LK" peptide, sequence: Ac-LKK[^{13}C]LLKL[^{15}N]LKKLLKL, 4.2 Å distance). Next, the REDOR experiment was applied to three samples of labeled histatin-5: [^{13}C]Ala$_4$-[^{15}N]His$_8$ hsn-5, [^{13}C]Tyr$_{10}$-[^{15}N]Phe$_{14}$ hsn-5, and [^{13}C]His$_{19}$-[^{15}N]Gly$_{23}$ hsn-5. Because of their physiological relevance, hydrated samples were investigated but the work was done at low temperature to enhance the poor sensitivity observed at room temperature, presumably due to some dynamic phenomena interfering negatively with the cross polarization (CP) efficiency.

The results, obtained at a temperature of about – 40ºC, indicated that the $^{13}C/^{15}N$ spin pair dipolar interactions, and thereby distances, in all three peptides were close to or beyond the detectable limits of REDOR. Consequently, the hydrated and bound peptides did not appear to adopt a α-helical secondary structure.

In parallel, the DRAWS (Dipolar Recoupling with A Windowless Sequence) (Gregory et al. 1995) experiments performed at the UW to determine distances between two ^{13}C carbonyl labels in adjacent amino acids (residues i and i+1) of bound and lyophilized histatin-5 confirmed the REDOR findings. The two $^{13}C_{1,i}$- $^{13}C_{1,i+1}$ reported distances of about 3.2 Å correlated with an extended backbone conformation of the peptide.

Backbone Dynamics of Bound and Hydrated Histatin-5

Interest in the subject of the dynamics developed as the structural characterization of histatin-5 was being undertaken. As mentioned above, at room temperature, lower signal sensitivities seemed to indicate weak CP efficiencies. ^{13}C $T_{1\rho}$ measurements became of interest with the warning that these quantities depend on dipolar couplings and chemical shift anisotropies. However, performing the experiments on peptides labeled at various nuclear positions of a given chemical type (backbone carbonyl carbons here) allows the results to be meaningfully compared. Experiments were performed at the EMSL on hydrated and bound histatin-5 using unlabeled and ^{13}C carbonyl backbone labeled samples. Results obtained with various spinning speeds and contact times were compared and lead to the characterization of some peptide backbone dynamics. The results are now in their final form before submission for publication (Cotten et al. in press) therefore our conclusions will be only briefly outlined here. The peptide was found to exhibit some detectable yet slow dynamics in a quite even fashion all along its backbone. In comparison, the first five tightly bound amino acids of statherin, an acidic salivary biomineralization protein, appear static on the NMR time scale while the carboxylic end of this peptide is much more dynamic (Long et al. 2001). The project with histatin-5 is now moving forward with more direct studies of peptide-mineral interactions, including distance measurements between side chains and the hydroxyapatite surface.

We wish to thank the outside reviewers and EMSL staff for their continued support.

References

Brewer, D, and G Lajoie. *Rapid Commun. Mass Spectrom.*, **14**, 1736-1745 (2000).

Cotten, M, PS Stayton, and GP Drobny (in press).

Gregory, DM, DJ Mitchell, JA Stringer, S Kiihne, JC Shiels, J Callahan, MA Mehta, and GP Drobny. *Chem. Phys. Letters*, **246**, 654-663 (1995).

Gullion, T, and J Schaefer. *J. Mag. Reson,* **81**, 196-200 (1989).

Gusman, H, U Lendenmann, J Grogan, RF Troxler, and FG Oppenheim. *Biochim. Biophys. Acta*, **1545**, 86-95 (2001).

Long, JR, WJ Shaw, PS Stayton, and GP Drobny. *Biochem.*, **40**, 15451-15455 (2001).

Solid-State NMR Characterization of Alkali Incorporation into Synroc and its Constituent Phases

JV Hanna,[(a)] ML Carter,[(a)] ER Vance[(a)] and AS Lipton[(b)]
(a) Lucas Heights Research Laboratories, Australia
(b) Pacific Northwest National Laboratory

Synroc is a titanate based multiphase ceramic developed for the immobilization of Purex-type high-level waste from spent nuclear fuel reprocessing. The main constituent phases are zirconolite ($CaZrTi_2O_7$), perovskite ($CaTiO_3$), hollandite ($Ba(Al,Ti)_2Ti_6O_{16}$) and reduced rutile (TiO_2). It can accommodate nearly all fission products and actinides from high level waste in dilute solid solution. In addition to the complete multiphase product, there has been a large effort directed towards the design and synthesis of the individual channel structured components (namely zirconolite and hollandite) to study the viability of these highly ordered phases as wasteforms in their own right. In particular, hollandite has been thoroughly demonstrated as the synroc host of large fission product cations such as Cs^+ and Ba^{2+} (Carter et al. 2002, 2003); however, these studies have focussed primarily on Cs incorporation and its associated leach properties. This study has now been extended to the introduction of smaller alkalis such as Rb^+, K^+, and Na^+ as channel species; as with the abovementioned studies of Carter et al. the approach now undertaken is to evaluate this incorporation within a pure hollandite matrix rather than from the more complex synroc mixture.

The crystal structure of synroc-type hollandite has been the subject of many investigations. The hollandite group of minerals has the general formula $A_xB_yC_{8-y}O_{16}$. The B and C cations are surrounded octahedral configurations of oxygen. Each of these $(B,C)O_6$ octahedra share two edges to form paired chains running parallel to the *c* axis. The large A cations are located in these tunnels. In synroc-type hollandite, the A position is occupied by Ba^{2+}, Cs^+, Rb^+, K^+, and Na^+ (potentially), the B position by Al^{3+} and Ti^{3+}, and the C position by Ti^{4+}. This invokes the nominal general formula for synroc hollandite as being $[Ba_x(alkali)_y][(Ti,Al)^{3+}{}_{2x+y}Ti^{4+}{}_{8-2x-y}])O_{16}$.

In contrast to ^{133}Cs solid-state NMR studies of $[Ba,Cs][(Ti,Al)_2Ti_6O_{16}]$ which were undertaken with MAS techniques, the solid-state NMR studies of the K and Rb analogues must be performed as broadline (static) experiments at the highest available fields. The overall second order quadrupolar broadening on the central transition spectra of both ^{39}K and ^{87}Rb in these systems was too great to permit an optimal narrowing of these resonances by MAS methods. The low frequency of the K experiments and the excessive linewidths of the Rb resonances (coupled with the often low K and Rb substitution by weight in some samples) necessitated these studies be performed at the highest available field strength (18.8 T). Figure 1 shows the ^{39}K static NMR spectra acquired with the solid-echo experiment. From Figure 1(a) the sample $[K_{1.5}][(Al_{1.5}Ti_{0.5})Ti_6O_{16}]$ exhibits a well defined ^{39}K resonance with $\eta \sim 0$, suggesting that the K^+ ions in the channels are highly ordered. This result appears to be insensitive to the sample cooling rate upon firing at ~1400°C. Figure 1(b) shows the ^{39}K static NMR spectrum of $[Ba_{0.5}K_{0.5}][(Al_{1.5}Ti_{0.5})Ti_6O_{16}]$ fabricated under normal cooling conditions (~5°C/min). The lack of well-defined features on this resonance indicates that

very little (or no) ordering has occurred in the channel sites with respect to mixed Ba/K speciation that now dominates these positions. However, upon a much slower cooling rate of ~0.1°C/min, Figure 1(c) shows that order can be introduced within the mixed K/Ba channel occupancy, with a well defined $\eta \sim 1$ lineshape emerging.

The Rb analogues to the above systems exhibit quite different behaviour. Irrespective of the cooling rate employed in their fabrication, samples such as $[Rb_{1.5}][(Al_{1.5}Ti_{0.5})Ti_6O_{16}]$ and $[Ba_{0.5}Rb_{0.5}][(Al_{1.5}Ti_{0.5})Ti_6O_{16}]$ show no inclination to order within their respective pure Rb or mixed Rb/Ba channel occupancies. This phenomenon can be observed from Figures 2(a) and 2(b) which show the static ^{87}Rb NMR spectra of $[Rb_{1.5}][(Al_{1.5}Ti_{0.5})Ti_6O_{16}]$ and $[Ba_{0.5}Rb_{0.5}][(Al_{1.5}Ti_{0.5})Ti_6O_{16}]$, respectively. These central transition spectra exhibit poorly formed singularities on the quadrupolar dominated lineshapes and are indicative of residual intrinsic disorder. This contrasts markedly with the K case and is attributed to the comparitively smaller ionic radius of K^+ and the greater ease with which it can thermally reposition within the hollandite channels, as opposed the much larger Rb^+ ions.

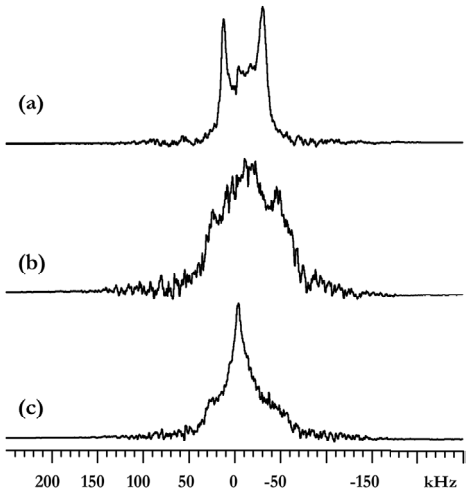

Figure 1. Static ^{39}K spectra acquired at 18.8 T.

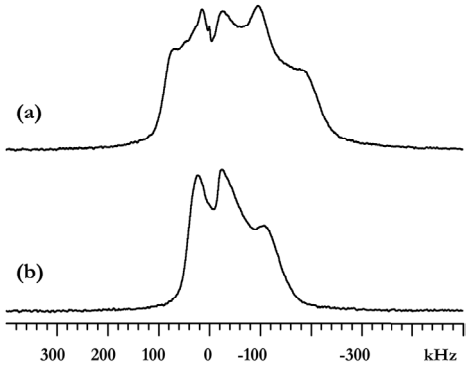

Figure 2. Static ^{87}Rb spectra acquired at 18.8 T.

References

Carter, ML, ER Vance, DRG Mitchell, JV Hanna, Z Zhang, and E Loi. Fabrication, characterization and leach testing of hollandite, $(Ba,CS)(Al,Ti)_2Ti_6O_{16}$. *J. Mater. Res.*, **17**, 2578-2589 (2002).

Carter, ML, JV Hanna, and ER Vance. A structural and spectroscopic comparison between the $(Ba,Cs)(Al,Ti)_2Ti_6O_{16}$ and $(Ba,Cs)(Ga,Ti)_2Ti_6O_{16}$ systems. *J. Mater. Res.* (in press).

Solution Structure of the Hypothetical Nudix Protein DR0079 From the Extremely Radiation-Resistant Bacterium *Deinococcus radiodurans*

GW Buchko,[(a)] S Ni,[(a)] SR Holbrook,[(b)] and MA Kennedy[(a)]
(a) Pacific Northwest National Laboratory
(b) Lawrence Berkeley National Laboratory, Berkeley, California

The bacterium *Deinococcus radiodurans* is able to withstand high doses of ionizing and UV radiation that are lethal to virtually all other organisms (Battista 1997). It has been suggested that this resistance to radiation and to other DNA-damaging agents (including hydrogen peroxide and mitomycin C) may be due to unusually efficient DNA repair mechanisms (Minton 1994). Consequently, *D. radiodurans* is one of the leading candidates for the bioremediation of radioactive waste and a subject for the study of DNA repair mechanisms.

The complete genome of *D. radiodurans* has been sequenced (White et al. 1999). Analysis of this sequence reveals a full collection of genes with potential DNA repair activities, essentially all of which have functional homologues in other procaryotes. Interestingly, these hypothetical DNA repair genes exhibit a high amount of redundancy that includes 21 genes that have sequence homology with the Nudix family of polyphosphate pyrophosphohydrolases. Nudix proteins are found in all organisms and are identified by the consensus sequence $GX_5EX_7REUXEEXGU$ (where U = I, L, or V and X = any amino acid) that forms part of the catalytic site for the hydrolysis of a **NU**cleoside **DI**phosphate linked to some other moiety, **X**. Their primary functions are to sanitize the cell by reducing the level of potentially mutagenic and/or toxic compounds and the accumulation of biochemical intermediates. While more than 450 putative Nudix proteins have been identified in genomes on the basis of the Nudix consensus sequence, few Nudix protein structures have been determined. For those few structures that have been determined, beyond the conserved cataylic core there is a considerable variation in the peripheral structure and oligomerization state. To better understand the relevance, function, and mechanisms of the Nudix family of proteins, and to better understand the roles played by the hypothetical *D. radiodurans* Nudix proteins in radiation-resistance, we have targeted the 21 hypothetical Nudix proteins for structure determination. Using the NMR facilities at the Environmental Molecular Sciences Laboratory, we collected data that allowed us to determine the solution structure for the hypothetical *D. radiodurans* Nudix protein DR0079, a 171 residue, 19.3 kDa protein.

Solution structure of DR0079

Dual ^{13}C- and ^{15}N-labelled NMR samples of DR0079 were prepared as previously been described (Buchko et al. in press; Holbrook et al. in press). A suite of NMR experiments was employed to assign 95% of the backbone and the majority of the side chain ^{1}H, ^{13}C, and ^{15}N resonances (Buchko et al. in press) and these values have been deposited in the BioMagResBank (accession number BMRB-5570). Using the ^{1}H assignments, distance restraints were obtained from 3-D ^{15}N-edited NOESY and 4-D ^{13}C-edited NOESY

experiments and used to calculate an ensemble of solution structures using distance geometry/simulated annealing protocols (Xplor v3.840). Figure 1 summarizes the average structure of an ensemble of structures calculated for DR0079. The core is composed of a 4-strand mixed β-sheet interconnected by a loop-helix-loop motif. The latter element contains the 23-residue signature motif of Nudix proteins (G70-V92). On opposite ends of this core structure are 18 N-terminal residues that contain an anti-parallel β-sheet and 23 C-terminal residues that form an helix-turn-helix motif. Using the three-dimensional structure of DR0079, it will now be possible to determine, in detail, metal and substrate binding sites.

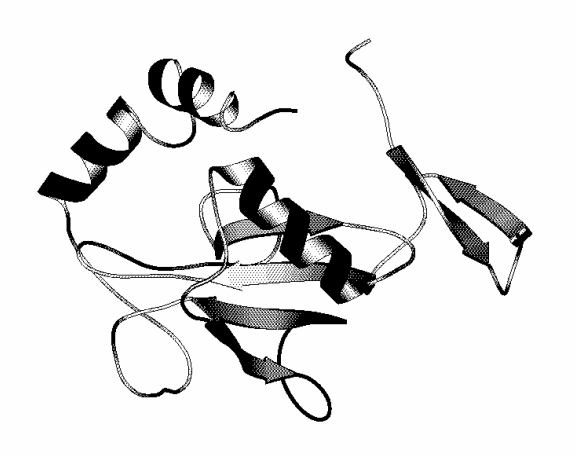

Figure 1. Ribbon representation of the average solution structure for DR0079. The helix in the center of the structure contains the signature Nudix motif and adopts a loop-helix-loop fold.

References

Battista, A. AGAINST ALL ODDS: The survival strategies of *Deinococcus radiodurans*. *Annual Review of Microbiology*, **51**, 203-224 (1997).

Buchko, GW, S Ni, SR Holbrook, and MA Kennedy. ^{1}H, ^{13}C, and ^{15}N NMR assignments of the hypothetical Nudix protein DR0079 from the extremely radiation-resistant bacterium *Deinococcus radiodurans*. *Journal of Biomolecular NMR* (in press).

Holbrook, EL, U Schulze-Gahmen, GW Buchko, S Ni, MA Kennedy, and SA Holbrook. Purification, crystallization and preliminary X-ray analysis of two Nudix hydrolases from *Deinococcus radiodurans*. *Acta Crystallographica, Section D: Biological Crystallography* (in press).

Minton, KW. DNA repair in the extremely radioresistant bacterium *Deinococcus radiodurans*. *Molecular Micribiology*, **13**, 9-15 (1994).

White, O et al. Genome sequence of the radioresistant bacterium *Deinococcus radiodurans* R1. *Science*, **286**, 1571-1577 (1999).

NMR Structural Investigations of the Breast Cancer Susceptibility protein, BRCA1

P Brzovic,[(a)] DW Hoyt,[(b)] and RE Klevit[(a)]
(a) University of Washington, Seattle
(b) Pacific Northwest National Laboratory

The breast and ovarian cancer tumor suppressor protein supports a number of fundamental cellular processes. Its absence during embryogenesis is lethal. Loss of function can result in breast or ovarian cancer. A growing body of literature suggests that BRCA1 interacts with at least 25 different macromolecules to function in processes such as the cellular response to DNA damage, homologous recombination, transcriptional regulation, and ubiquitination. A complete picture of the cellular role of BRCA1 requires a detailed understanding of both the function and the structure of the protein and its interacting partners.

BRCA1 is a large and complicated protein that undoubtedly comprises a multiplicity of functional domains. This work has focused on the N-terminal RING domain of BRCA1. Encompassing only 110 residues, this remarkable region of BRCA1 is the site of numerous mutations found in families genetically predisposed to breast and ovarian cancer. A number of different protein partners have been identified which specifically interact with this domain. These proteins include the N-terminal RING domain of BARD1, a protein that also interacts with the mRNA polyadenylation factor CstF-50. Of particular interest is the recent demonstration that the BRCA1 RING domain exhibits activity as an E3 ubiquitin ligase. Protein ubiquitination provides a powerful regulatory mechanism for controlling pathways that include cell-cycle progression and transcriptional regulation.

As E3-ligases, RING domains are thought to facilitate the specificity of ubiquitination reactions by binding both a ubiquitin conjugating enzyme (E2) covalently activated with ubiquitin and specific proteins targeted for ubiquitination. The RING domain of BRCA1 has been shown to have E3 ligase activity only in conjunction with the E2 enzyme UbcH5 and only when complexed with the RING domain of BARD1. The BRCA1-BARD1 complex represents a novel RING-RING E3-ligase (Figure 1). Structural characterization of the interaction of the BRCA1/BARD1 heterodimer complex with its various protein partners promises to yield important insight regarding mechanisms of ubiquitination, the function of the BRCA1 RING domain, and also further our understanding of the molecular mechanism underlying the deleterious structural and functional consequences of BRCA1 cancer pre-disposing mutations.

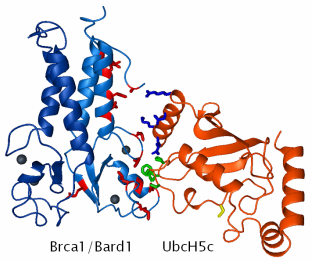

Figure 1. The BRCA1-BARD1 complex with the E2 enzyme UbcH5.

This is a unique and challenging system for studying protein-protein interactions by NMR. It involves characterizing the interactions between at least four different protein components with a total molecular weight approaching 52 kD. Understanding how a functional complex is assembled requires multiple NMR approaches, including chemical shift mapping and NOESY-based experiments to observe intermolecular NOE's. Of course, complete backbone and side-chain assignments must be available to interpret these data and calculate structure(s).

An important milestone in this ongoing work was the determination of the structure of the BRCA1-BARD1 heterodimer using data collected at EMSL (Brzovic et al. 2001). Over the last year, work at EMSL has allowed us to map protein-binding surfaces that govern the interaction between BRCA1/BARD1, UbcH5 and Ub using chemical shift mapping techniques. These data have revealed 1) that although there are two RING domains available, UbcH5c interacts only with the BRCA1 subunit, 2) a non-covalent Ub binding surface on UbcH5c important for activity and 3) that different E2 proteins recognize and bind to the same surface of BRCA1, yet not all exhibit activity in BRCA1-mediated ubiquitination reactions. These data provide valuable information as to what determines an active E3-E2 pairing. A manuscript describing these results, "Binding and Recognition in the Assembly of an Active BRCA1-BARD1 Ubiquitin Ligase Complex" is in the final stages of revision for publication in PNAS. We have continued this work with complementary experiments to map the surfaces of E2 proteins that recognize BRCA1. Interpretation of these experiments required complete backbone assignments, which also have been accomplished during the last year.

We have discovered that the binding of UbcH5c to the BRCA1-BARD1 heterodimer alters the chemical shift of residues at the UbcH5c active site, a distance of over 15Å. Secondly, we have identified important potential E2 catalytic residues. with unusual NMR properties. Mutation of one such residue dramatically reduces the activity of UbcH5c in BRCA1-mediated ubiquitin-transfer reactions. Data collected at EMSL reveal that the resulting NMR spectral changes are minor and restricted to the region immediately surrounding the mutation site. These studies show that the interaction of the mutant UbcH5c with other proteins is not significantly altered and this mutant is still capable of being charged with Ub at its active site by an E1 ubiquitin-activiating enzyme. This mutant promises to be a valuable aid to study the interaction of BRCA1/BARD1 with an E2 conjugated with Ub.

Our studies at EMSL have uncovered a non-covalent binding site for Ub on a surface of UbcH5c opposite the active site. A single mutation within this site is sufficient to eliminate poly-ubiquitination activity *in vitro*. Though the affinity of this site for Ub is weak (Kd ~ 1μM), we have been able to use the high field instruments at EMSL to observe intermolecular NOE's (Figure 2), which will allow determination of the structure of the complex and help us understand why this interaction is necessary for poly-ubiquitination activity.

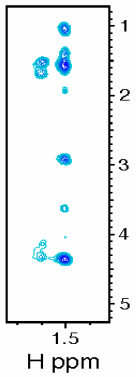

Figure 2. Intermolecular NOE crosspeaks between UbcH5c and Ub collected at 800 MHz.

Deciphering the protein-protein interactions in this system is a challenging problem particularly suited to NMR approaches. The nature of the interactions essentially precludes use of X-ray crystallography. Due to the size and nature of the complexes, this work benefits tremendously from the high-field instruments available at EMSL. Collection of data with high sensitivity and resolution has allowed us to make substantial progress during the last year and we anticipate similar progress during the next year.

Publications resulting from work at EMSL

Brzovic, PS, JR Keeffe, H Nishikawa, K Miyamoto, D Fox, M Fukuda, T Ohta, and RE Klevit. Binding and Recognition in the Assembly of an Active BRCA1-BARD1 Ubiquitin Ligase Complex, *Proc. Natl. Acad. Sci.* (in press).

Brzovic PS, P Rajagopal, DW Hoyt, MC King, and RE Klevit. Structure of a BRCA1-BARD1 heterodimeric RING-RING complex. *Nat Struct Biol.* (10):833-7 (2001).

Brzovic PS, JE Meza, MC King, and RE Klevit. BRCA1 RING domain cancer-predisposing mutations. Structural consequences and effects on protein-protein interactions. *J Biol Chem.,* **276**(44):41399-406 (2001).

Pulsed EPR Investigations of the Cytochrome bc_1 and b_6f Complexes

DM Kramer[(a)] and AG Roberts[(a)]
(a) Washington State University, Pullman

Our work with EMSL focused on the mechanism of the cytochrome (cyt) bc_1 and b_6f complexes, key components of mitochondrial and photosynthetic electron transfer chains. These complexes are important for energy transduction in many organisms, including humans. Under certain conditions, these complexes can also produce the detrimental reactive oxygen species superoxide, which can contribute to diseases. Our aim is to understand the mechanism of these complexes, as well as the conditions and the basis for superoxide production. Access to the EPR facilities at EMSL, and perhaps more importantly, the expertise and deep insights of Dr. Michael K. Bowman at EMSL, were vital to this work

The cytochrome (cyt) *bc* complexes constitute a major part of the energy transduction machinery in many living cells. They catalyze the transfer of electrons from reduced quinone (ubihydroquinone or ubiquinol in mitochondria, plastoquinol in chloroplasts and menaquinol in many bacteria) to a soluble protein (cyt *c*, plastocyanin or, in some cases a high-potential iron sulfur protein, or HIPIP). This transfer is tightly coupled to the pumping of protons across the membrane that contains the complex and the resulting electrochemical potential of protons drives the synthesis of ATP via a chemiosmotic circuit. The cyt *bc* complexes are broken into two classes: bc_1 and b_6f types, although forms intermediate between the bc_1 and b_6f complexes have been found in some bacteria. Both cyt bc_1 and b_6f complexes contain four redox-active, metal centers: one heme *c*, one Rieske-type Fe_2S_2 center, and two *b*-type hemes. These metal centers are found in three proteins: heme *c* in cyt c_1 (or cyt *f* in b_6f); the Rieske Fe_2S_2-protein (ISP); and the *b* hemes in a single cyt *b* (or cyt b_6 in b_6f).

The working model for most research in this area is the Q-cycle, where two protons are pumped across the energetic membrane for each electron transferred from quinol to a high potential acceptor. The electron transfer is a bifurcated process, as illustrated in Figure 1. One electron from the hydroquinone (or quinol) in site Q_o (labeled SQ_o in Figure 1) is transferred to the Rieske Fe_2S_2 center while the other is forced to flow through a chain of two cyt *b* hemes to reduce a quinone in site Q_i (labeled SQ_i in Figure 1). Both protons from site Q_o are ultimately released on the *p*-side of the membrane while the quinone at the Q_i site picks up two protons from the *n*-side of the membrane. Thus, since the bifurcation of the electron flow at the Q_o site allows only one quinol electron to pass to the high-potential electron acceptor (i.e., cyt *c* in

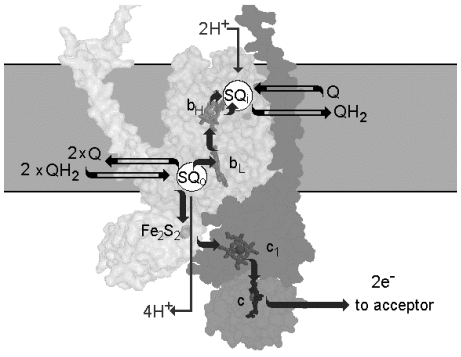

Figure 1. The Q-cycle for the cyt bc_1 complex.

mitochondria, plastocyanin or cyt c_6 in chloroplasts), it doubles the expected number of protons pumped per electron and accounts for the high efficiency of energy transduction by the *bc* complexes.

The recent publication of high-resolution X-ray structures of mitochondrial cyt bc_1 complexes has greatly accelerated progress in understanding the function of these enzymes. One notable feature of the crystal structures is a variation in the position of the "head" (or hydrophilic extension) of the ISP. The presence of two distinct ISP conformations led to the "domain movement" hypothesis where the ISP pivots back and forth to "gate" electron transfer, forcing the two electrons on the quinol to be transferred through different pathways. In one conformation, quinol is bound at the Q_o site and transfers one electron to the Fe_2S_2 center. Further transfer of this electron is prevented because the ISP in this conformation is distant (~31Å) from cyt c_1. Thus, the remaining semiquinone electron is transferred to the low potential cyt b_L then to cyt b_H and finally to a quinone or semiquinone bound at the Q_i site. Only after full oxidation of quinol does the ISP pivot and make close contact with cyt c_1, allowing electron transfer to mobile cyt *c*. In collaboration with EMSL, we have confirmed such motion EPR measurements on partially oriented samples of the cyt b_6f complex. A further significant advance was the discovery that found that that certain metal ions inhibit the cyt b_6f complex by binding to cyt *f* and interfering with ISP domain movements (Figure 2).

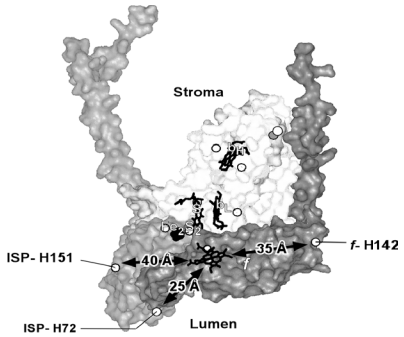

Figure 2. A model of the complete cyt b_6f complex based on X-ray structures of the cyt *f* and ISP domains and on homology with the cyt bc_1 structures (See Figure 3), which shows the location of bound Cu^{2+} determined by pulsed EPR.

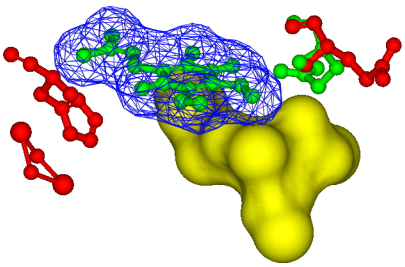

Figure 3. Characterization of the partial reactions observed in the presence of certain inhibitors suggests a structure for the substrate bound to the cyt bc_1 complex. Shown is a hypothetical structure of ubiquinol (blue mesh) co-bound to residues of the substrate binding site (red/green) in the presence of the inhibitor mucidin (yellow).

In research supported by NSF (IBN-9817980) and DOE (DE-FG03-98ER20299), we have shown that, regardless of the *in vivo* energy status of the plant, electron transfer through the cyt b_6f complex appears tightly coupled to the pumping of protons. Our current work focuses on determining why this coupling is so tight. One of the key obstacles in answering this question has been the lack of knowledge about how substrate interacts with the active site. We have made two significant contributions towards defining the substrate-binding site, again in collaboration with Michael K. Bowman at EMSL. First, we have shown that two quinone analogs can bind simultaneously to the site. Secondly, we have been able to define the structural bounds of substrate binding by probing the partial reactions of the enzyme in the presence of a series of different inhibitors (Figure 3).

Reference

Muller, F, AR Crofts, and DM Kramer. Multiple Q-cycle bypass reactions at the Q_o-site of the cytochrome bc_1 complex. *Biochemistry*, **41**:7866-7874 (2002).

Rao BK, S, AM Tyryshkin, AG Roberts, MK Bowman, and DM Kramer. Inhibitory copper binding site on the spinach cytochrome *b6f* complex: Implications for Q_o site mechanism. *Biochemistry*, **39**:3285-3296 (2000).

Roberts, A, and DM Kramer. Inhibitor 'double-occupancy' in the Q_o pocket of the chloroplast cytochrome b_6f complex. *Biochemistry*, **40**:13407-13412 (2001).

Roberts, A, and DM Kramer. Inhibitor 'double-occupancy' in the Q_o pocket of the chloroplast cytochrome b_6f complex. *Biochemistry*, **40**(45):13407-13412 (2001).

Roberts, AG, S Rao BK, and DM Kramer. Metal ions as probes of 'Rieske' ISP domain movements, in *PS2001 Proceedings*. CSIRO Publishing: Collingwood, Vic. Australia. p. 1-4 (2001).

Aluminum Coordination Environments in Mesoporous Alumina

G Burnside,[(a)] L Wilcox,[(a)] R Shekhawat,[(a)] R Hawk,[(a)] M Mazumder,[(a)] D Lindquist,[(a)] and S Burton[(b)]

(a) University of Arkansas at Little Rock

(b) Pacific Northwest National Laboratory

Mesoporous aluminas are valued in catalysis because they exhibit a combination of properties that allow both long life and activity. The surface area, acidity, stability, and pore size of the alumina influence properties. Of particular interest are the coordinatively unsaturated environments of four coordinate (Al^{IV}) and five coordinate (Al^{V}) aluminum that comprise the Lewis acid sites (Coster and Fripiat 1993). MAS ^{27}Al NMR provides perhaps the best direct measure of coordination environments. Synthetic aluminas, including those produced commercially, contain Al^{IV} and Al^{VI}, but little or no Al^{V}. Improved catalysts and new applications are likely to result from aluminas with more Al^{V}. NMR experiments at PNNL in January 2002 on the Varian Infinity 300 MHz instrument confirmed the presence of Al^{V} in alumina prepared by a new method developed at the University of Arkansas at Little Rock (UALR).

Figure 1 shows side by side ^{27}Al MAS NMR comparison of UALR alumina A3, and a commercial alumina (Alcoa Hi-Q 30) B. The resonances for Al^{IV}, Al^{V}, and coordinatively saturated Al^{VI} occur at about 65, 35, and 0 ppm respectively. The top two spectra of both aluminas in Figure 1 show similar ratios of Al^{IV} and Al^{VI} environments. The stability of Al^{IV} over such a large temperature range is characteristic of transition aluminas. The spectra for B (Alcoa Hi-Q 30 alumina) in Figure 1 are consistent with the phase changes observed by independent powder x-ray diffraction studies. Only the Al^{VI} resonance is discernible for the bottom two B spectra since B is a pseudoboehmite. Conversion of pseudoboehmite to γ-Al_2O_3 at 500°C coincides with the emergence of Al^{IV} in the B spectra. The A3 alumina exhibits a substantial fraction of Al^{V} after heating to 300°C, but which is lost after heating to 500°C in air.

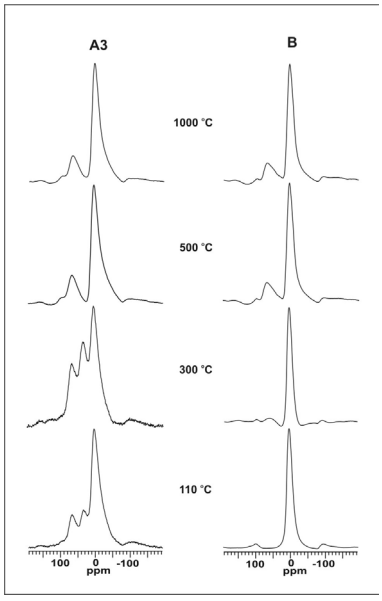

Figure 1. ^{27}Al MAS NMR of aluminas heated in air. The A3 spectra are from an alumina synthesized at UALR, whereas B corresponds to a commercial boehmite.

Interestingly, another "A3" sample heated in a steam atmosphere rather than air exhibited substantial Al^{V} after 500 °C. These results are shown in Figure 2.

Based on these unusual findings, we requested and were alloted time for another NMR study on the effects of steam atmosphere on Al^{V} in the aluminas. The measurements are underway at the time of this writing and will be reported in future.

One publication has resulted from our initial NMR studies (Wilcox et al. 2003) and we look forward to publishing the results of the current steam calcination experiments. In addition, the NMR data gathered to date is being used to optimize preparation of catalysts for emission control studies for automobile catalytic converter applications at UALR. In addition, we are submitting a proposal to EMSL to investigate the aluminum coordination environments in lanthanum stabilized alumina and in hydrotalcite, both synthesized using modifications of the synthetic method developed for alumina.

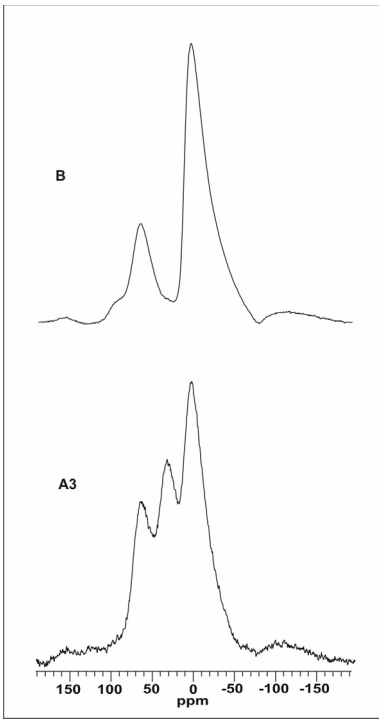

Figure 2. ^{27}Al MAS NMR of aluminas heated in steam to 500 °C.

References

Coster, D, and JJ Fripiat. Memory Effects in Gel-Solid Transformations: Coordinatively Unsaturated Al Sites in Nanosized Aluminas, *Chemistry of Materials*, **5**, 1204-1210 (1993).

Wilcox, L, G Burnside, B Kiranga, R Shekhawat, MK Mazumder, RM Hawk, DA Lindquist, and SD Burton. Porous Alumina Prepared from Diethylaluminum Amide, Acetone, and Water. *Chemistry of Materials*, **15**, 51-56 (2003).

High-Field Solid-State NMR Studies of Weathered Specimen Kaolinite Clays

KT Mueller[(a)] and GS Crosson[(a)]
(a) Penn State University, State College, Pennsylvania

Interactions with natural soil particles govern the mobility of radionuclides in the saturated and unsaturated zones at Department of Energy (DOE) sites affected by radioactive contamination. High surface area aluminosilicate clay minerals are recognized as important radionuclide sorbents. Clay minerals are prone to weathering-induced transformations during exposure. To better understand fundamental processes taking place in the vadose and saturated soil environments, studies of specimen clay samples must be undertaken. We are currently studying the transformation of clays under specific chemical conditions that mimic the composition of the contaminant solutions (Choi et al. in press). The DOE EMSP program, via grant DE-FG07-99ER15012, currently supports this work.

Kaolinite ($Al_2Si_2O_5(OH)_4$) consists of a gibbsite-like aluminum hydroxide sheet and a tetrahedral silicate sheet held together via electrostatic interactions with proton and oxygen moieties, and it is present along with other clay minerals at contaminated DOE sites. This mineral has a pH dependent charge resulting from protonation and deprotonation reactions of silanol and aluminol groups. At the high pH (~14) of the contaminant solutions, all of these groups are expected to be deprotonated, thus facilitating the absorption of ^{137}Cs and ^{90}Sr along with a mineral transformation to other aluminosilicate phases such as zeolites and short-range ordered aluminum and silicon containing phases, which could retard the mobility of contaminant radionuclei. The potential for mineral transformation to new aluminum and silicon containing phases necessitates a thorough study of the aluminum environments in weathered systems. We are using high-field ^{27}Al solid-state NMR to further this study. The objectives of this research are 1) to observe and identify neo-phases formed in weathered kaolinite systems as a function of contact time with a synthetic leachate solution and also as a function of (non-radioactive) Cs and Sr initial concentrations, and 2) to resolve, characterize, and quantify the aluminum environments in select weathered samples.

Thus far, a number of single resonance ^{27}Al NMR experiments have been performed on specimen kaolinite samples exposed to a synthetic tank waste leachate solution composed of 2.0 M Na^+, 1 M NO_3^-, 1 M OH^-, a total aluminum concentration of 0.05 M, and three different initial concentrations of Cs and Sr (10^{-5} M, 10^{-4} M, 10^{-3} M). Magic-angle spinning (MAS) ^{27}Al NMR experiments were performed at magnetic field strengths of 7.0 T, 9.4 T, and 11.7 T in the Penn State NMR Facility (located in the Department of Chemistry) and in the laboratory of Professor Mueller. At 7.0 T, a single resonance near 4 ppm is observed in the spectrum of pure (unreacted) kaolinite; this resonance is assigned to six-coordinate aluminum. Upon reaction, the most noticeable new feature at 7.0 T (observed as a function of time for all three initial concentration conditions studied) is the uneven growth of an asymmetrical resonance at 50 to 65 ppm. This spectral change indicates the formation of new phase(s) containing tetrahedral aluminum sites. The asymmetrical nature of the tetrahedral resonance suggests the presence of multiple phases.

Preliminary diffraction studies have been performed on all of the samples; the identities of crystalline phases containing tetrahedral aluminum are most likely zeolitic in nature. In an effort to separate, identify, and quantify the various aluminum environments, all samples were then run at 9.4 T and 11.7 T magnetic field strengths. Multiple field MAS spectra (normalized to the intensity of the tetrahedral resonance) are presented for reacted clays (190 days at an initial concentration of Cs and Sr of 10^{-5} M) in Figure 1. If the asymmetrical nature of the new resonance is due solely to second-order quadrupolar effects (and not multiple sites), it was expected that the resonance should only narrow. At 9.4 T and 11.7 T magnetic field strengths, the resonances not only become narrow but additional features appear which cannot be fully resolved. Regardless of the magnitude of the quadrupolar interaction, the interaction and its distribution should be reduced at higher magnetic field strengths leading to resolvable and assignable sites within our weathered systems. Thus, it became clear that one must obtain ^{27}Al spectra on these samples at the highest fields possible.

We were allotted four days of NMR time on the EMSL 750 MHz NMR system, and performed ^{27}Al MAS NMR experiments on standard reference samples, an unreacted kaolinite clay sample, and a matrix of 18 reacted samples (three different Cs and Sr concentrations, samples reacted for 30, 90, 190, and 369 days; and three different Cs and Sr concentrations, samples reacted for 190 and 369 days, and then subjected to an acidic ammonium oxalate wash to remove short-range ordered species). A sample spectrum is shown in Figure 1, demonstrating the enhanced and superior resolution in the tetrahedral region of the spectrum (near 60 ppm). Results are currently being quantified prior to publication, and concentrations as well as NMR parameters related to the specific Al environments are being calculated.

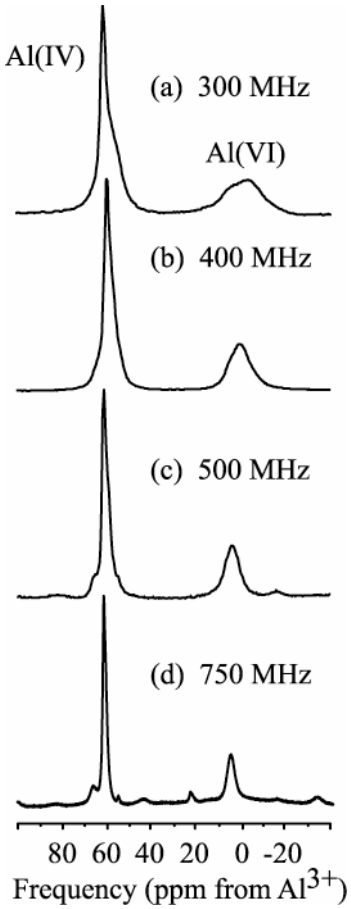

Figure 1. Single-pulse ^{27}Al MAS spectra of reacted kaolinite samples (190 days) at different magnetic field strengths (numbers listed are ^{1}H resonance frequencies). Spectrometer frequencies for ^{27}Al observation are (a) 77.48 MHz, (b) 104.25 MHz, (c) 130.19 MHz, and (d) 195.32 MHz. Spectra were recorded at spinning rates of (a) 14 kHz, (b) 14 kHz, (c) 10 kHz, and (d) 8 kHz. Spectral lines narrow with increasing field strength, indicating a reduction in second-order quadrupolar effects. Spectra features at all fields are consistent with the presence of six-coordinate aluminum in kaolinite and four-coordinate aluminum in zeolitic or other neophases.

References

Choi, S, J Chorover, G Crosson, MK Amistadi, and KT Mueller. Mineral transformation in colloidal kaolinite suspensions under tank waste leachate conditions. *Environ. Sci. Technol.* (in press).

Solid-state ^{67}Zn NMR Spectroscopic Studies and *ab initio* Molecular Orbital Calculations on a Synthetic Analogue of Carbonic Anhydrase

AS Lipton,[a] C Bergquist,[b] G Parkin,[b] and PD Ellis[a]
(a) W.R. Wiley Environmetal Molecular Sciences Laboratory
(b) Columbia University, New York City, New York

The principal motivation behind this research is the novel chemistry manifested by zinc and the associated biological significance of that chemistry. In zinc metalloproteins, the role of zinc can either be structural or catalytic. The structural role of zinc is dictated by its propensity to occupy tetrahedral sites rather than octahedral or pentacoordinate sites in metalloproteins. The catalytic properties often take advantage of the fact that the Zn^{2+} ion has an intermediate value of hardness or softness. This intermediate hardness introduces an element of flexibility into the Lewis acidity of the Zn^{2+} ion. One critical aspect of zinc chemistry of interest in bioinorganic chemistry involves the Zn-OH_2 functional group. Enzymes often use zinc to activate coordinated water towards deprotonation at close to neutral pH. For example, the conversion of the bound water to a hydroxide is central to the mechanism of action of carbonic anhydrase (Christianson and Fierke 1996). Depending upon the nature of the protein-derived ligands attached to the zinc, the water may require additional activation by interaction with the basic form of a proximal amino acid side chain. The Zn-OH_2 moiety is the principal catalytic functionality in the mechanism of action of the majority of zinc enzymes, and the water is activated by ionization, polarization, or poised for displacement depending upon the identity and spacing of the other coordinating ligands. In order to understand how these mechanisms are determined, it is first absolutely essential to understand how the coordination environment modulates the chemistry of zinc.

A long term goal of this research is to obtain a thorough understanding of the bioinorganic chemistry of zinc by investigating proteins and their synthetic analogues that are designed to mimic both the structure and function of the active sites of zinc enzymes. One of the vehicles to obtaining this objective is through the use of spectroscopy. Unfortunately, with a stable $3d^{10}$ electron configuration, the Zn^{2+} ion is not amenable to investigation by either UV/Vis or EPR spectroscopy. However, it has recently been demonstrated that solid-state ^{67}Zn NMR can be made practical by using cross-polarization (CP) methods in combination with low temperature (< 25K) and paramagnetic dopants (Lipton et al. 2001, 2002). It is essential to characterize the sensitivity of ^{67}Zn NMR parameters to subtle changes of structure in order to be able to relate these changes to specific structural/electronic effects. Therefore, in this work we have investigated the solid-state ^{67}Zn NMR spectroscopy of a more representative synthetic analogue of carbonic anhydrase, the tris(3-t-butyl-5-methylpyrazolyl) hydroborato zinc complex [$Tp^{Bu^t,Me}$]ZnOH, (Alsfasser et al. 1991) which not only possesses the requisite [ZnN_3O] motif but also reacts with CO_2 to generate a bicarbonate complex (Looney et al. 1993). Furthermore, studies on the halide derivatives [$Tp^{Bu^t,Me}$]ZnX (X= Br, Cl) have been carried out to determine the impact of a zinc substituent on the derived NMR spectroscopic parameters. These results are summarized in Table 1.

Table 1. Extracted parameters from the solid-state NMR lineshapes.

Parameters	$[Tp^{Bu^t,Me}]ZnBr$	$[Tp^{Bu^t,Me}]ZnCl$	$[Tp^{Bu^t,Me}]ZnOH$
σ_{iso} (ppm)	57.7	311.3	166.5
Cq (MHz)	9.5	12.3	30.5
η_q	0	0	0
$\Delta\sigma$ (ppm)	-374.9	-243.1	-301.2

Assuming the $[Tp^{Bu^t,Me}]$-Zn framework is similar for $[Tp^{Bu^t,Me}]ZnOH$, $[Tp^{Bu^t,Me}]ZnBr$, and $[Tp^{Bu^t,Me}]ZnCl$, the changes observed in Cq are due to the contributions from the bromide, chloride and hydroxide ligands. As the hydroxide species represents the largest ^{67}Zn quadrupole coupling reported to date, the question becomes why is this so dramatic a change from other zinc species studied? Since the changed in the electronegativities of the ligands can be viewed as incremental, one can conclude that the large change in Cq is more reflective of the shorter Zn-O bond than the electronic consequences of the changes in electronegativity.

To determine if this large Cq is reasonable we have performed *ab initio* molecular orbital calculations on $[Tp^{Bu^t,Me}]ZnOH$ to compare its predicted field gradient tensor with its experimental value and also compare the values with that of a proposed model for the active site of carbonic anhydrase, namely $[(MeImH)_3Zn(OH)]^+$. The simulated lineshapes are contrasted with the experimental spectrum in Figure 1.

The results of this work are currently in press and will appear in a upcoming issue of the Journal of the American Chemical Society.

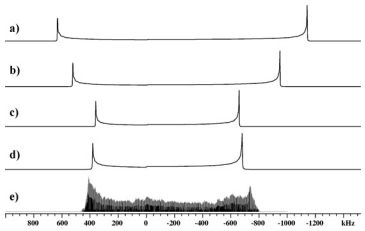

Figure 1. Predicted 9.4 T ^{67}Zn NMR spectra from *ab initio* MO theory contrasted with the experimental spectrum of $[Tp^{Bu^t,Me}]ZnOH$ where; (a) is from a fully RHF optimized geometry, (b) used the optimized RHF geometry and a single point MP2 calculation, (c) used a DFT optimized geometry, (d) is from an RHF optimized geometry on $[(MeImH)_3ZnOH]^+$, and (e) is the experimental spectrum of $[Tp^{Bu^t,Me}]ZnOH$.

References

Alsfasser, R, S Trofimenko, A Looney, G Parkin, and H Vahrenkamp. *Inorg. Chem.*, **30**, 4098-4100 (1991).

Christianson, DW, and CA Fierke. *Acc. Chem. Res.*, **29**, 331-339 (1996).

Lipton, AS, JA Sears, and PD Ellis. *J. Magn. Reson.*, **151**, 48 (2001)

Lipton, AS, TA Wright, MK Bowman, DL Reger, and PD Ellis. *J. Am. Chem. Soc.*, **124**, 5850-5860 (2002).

Lipton, AS, GW Buchko, JA Sears, MA Kennedy, and PD Ellis. *J. Am. Chem. Soc.*, **123**, 992-993 (2001).

Looney, A, R Han, K McNeill, and G Parkin. *J. Am. Chem. Soc.*, **115**, 4690-4697 (1993).

NMR Analysis of Methyl Groups in the 240kDa Arp2/3 Complex and Model Systems up to 560kDa

M Kreishman-Deitrick,[(a)] C Egile,[(b)] DW Hoyt,[(c)] JJ Ford,[(c)] R Li,[(b)] and MK Rosen[(a)]

(a) University of Texas Southwestern Medical Center at Dallas
(b) Harvard Medical School, Cambridge, Massachusetts
(c) Pacific Northwest National Laboratory

Signal-mediated rearrangements of the actin cytoskeleton are critical to many biological processes, including cell motility and morphology, bacterial and viral pathogenesis, and tumor metastasis. The 240 kDa Arp2/3 actin nucleation complex has emerged as a key regulator of these rearrangements, and has consequently become an important target of structural studies. Recent work has revealed that regulation of the actin nucleating activity of Arp2/3 complex by the Wiskott-Aldrich Syndrome protein (WASP) family proteins and filamentous (F-) actin is likely to involve a significant quaternary rearrangement in the complex. The nature of this conformational change and the binding modes of WASP proteins and F-actin are not currently understood.

Biomolecular solution NMR is an extremely powerful tool with which to study the structure, conformational dynamics, and ligand interactions of macromolecules and assemblies. A significant obstacle facing NMR spectroscopy of large systems is the rapid deterioration of NMR signals due to fast transverse relaxation. While most of the work to date has focused on NMR signals from protein amide groups, side-chain methyl groups offer a useful alternative spectroscopic probe in large systems. Methyl groups have several advantages over amides in terms of their utility in NMR spectroscopy. Methyl protons are not exchangeable with solvent, whereas amide proton line widths are inherently broadened by solvent exchange. ^{1}H-^{13}C correlation spectra are generally disperse and well resolved, and methyl ^{13}C and ^{1}H lines are inherently narrower as a result of rapid rotation of the three protons about the methyl symmetry axis. The presence of three protons per methyl group provides higher sensitivity and efficient longitudinal relaxation through intra-methyl dipolar interactions, resulting in short required T1 relaxation delays in NMR pulse sequences, even in systems highly deuterated at non-methyl positions. It has been shown that for ^{1}H,^{13}C(methyl)/ U-^{15}N,^{2}H-labeled samples of MBP (42 kDa) and DHNA (110 kDa), a simple $^{1}H/^{13}C$-HSQC spectrum of the methyl resonances is 3-fold and ~10-fold more sensitive, respectively, than a $^{1}H/^{15}N$-TROSY spectrum of the amides in the same sample. Methyl groups are also enriched in protein interiors and at protein-protein interfaces, and as with amide moieties, perturbation of methyl chemical shifts can be used to map ligand interactions.

Our time at EMSL has allowed us to establish the feasibility and scope of using methyl groups in NMR spectroscopy in molecules as large as 560 kDa. To establish the general utility of methyl groups in large systems, we used a test sample consisting of a 16 kDa protein suspended in a solution of 40% v/v glycerol. By exploiting the steep temperature dependence of glycerol solution viscosity, we were able to simulate a range of rotational correlation times (60–330ns), which corresponds to a molecular weight range of about 100 to 560kDa. The use of the high-field spectrometers available at EMSL allowed us to do a systematic, thorough analysis of $^{1}H/^{13}C$-HSQC spectra of this protein at a variety of

temperatures and at two different fields (see Figure 1). We find that signals from well-resolved methyl resonances can be detected in a 4.5-hour $^{1}H/^{13}C$-HSQC experiment on our 1.1mM model sample even at $\tau_C \approx 330$ns, and intense signals can easily be detected in a 100-hour spectrum of ~87μM Arp2/3 complex. These results indicate that protonated methyl groups will be powerful tools for the study of large macromolecular systems by NMR, even at significantly lower concentrations. We also took advantage of the high-field instruments at EMSL to compare the above methyl spectra with $^{1}H/^{15}N$-TROSY and CRINEPT-TROSY spectra on the same sample, and discovered that the methyl HSQC is in fact more sensitive than the amide experiments.

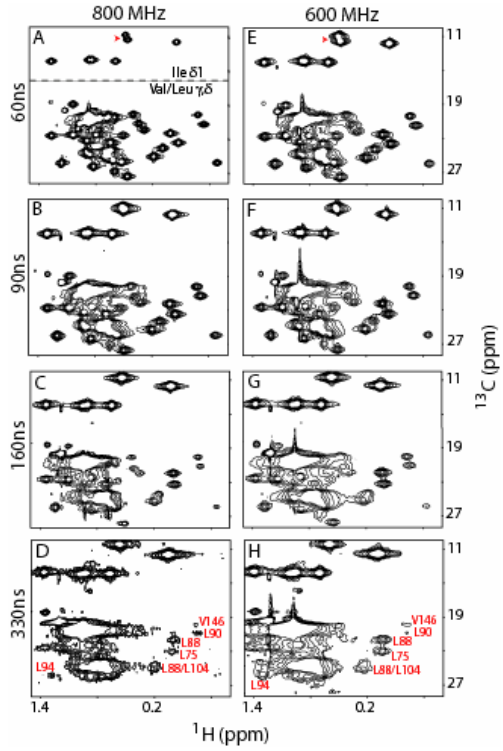

Figure 1. $^{1}H/^{13}C$-HSQC spectra of a 16 kDa protein in 40% v/v glycerol. Spectra were acquired at the fields indicated, and at the following temperatures: 25°C (panels A and E), 15°C (B and F), 0°C (C and G) and -10°C (D and H). Estimated τ_C values for each temperature are shown to the left of each row.

The work we have done at EMSL has established sidechain methyl groups as extremely sensitive probes for NMR spectroscopy of large molecules. The acquired $^{1}H/^{13}C$-HSQC spectra of Arp2/3 complex will allow us to dissect the interactions of this assembly with its activators. These studies will provide detailed insight into the mechanism of activation of this important cellular machine.

Publications resulting from work at EMSL

Kreishman-Deitrick, M, C Egile, D Hoyt, J Ford, R Li, and MK Rosen. NMR Analysis of Methyl Groups in the 240 kDa Arp2/3 Complex and Model Systems up to 560 kDa. Manuscript in preparation for submission to *Nature Structural Biology*.

Progress Towards Structural Determination of a Complex Membrane Protein, Diacylglycerol Kinase

CR Sanders[(a)] and FD Sönnichsen[(a)]

(a) Case Western Reserve University, Cleveland, Ohio

Prokaryotic diacylglycerol kinase (DAGK) is a homotrimeric integral membrane protein composed of 13 kDa subunits, with each subunit having three transmembrane helices (Figure 1). As a membrane protein, DAGK represents a class of proteins which is of enormous biological and biomedical importance, but which has proven largely refractory to structural determination by classical NMR and crystallographic methods. However, there has been recent and impressive progress in the area of membrane protein NMR, represented by the determination of monomeric beta barrel integral membrane porin structures (ca. 17 kDa) in detergent micelles by the Tamm/Bushweller, Wuthrich, and Kay labs. DAGK represents a target for NMR structural analysis which is at least one step beyond the porins in terms of difficulty because of its much larger size (40 kDa homotrimer) and because it is a largely helical protein. Determination of the structure of DAGK by solution NMR would be an important achievement for several reasons. If the structure of DAGK can be solved then it should be possible to also tackle the important G protein-coupled receptors, which tend to have roughly the same molecular weight and number of transmembrane segments as the DAGK homotrimer. These proteins are the target of at least 1/3 of all known drugs. Prokaryotic DAGK is itself of considerable interest for several reasons. It plays a critical function on a metabolic pathway (the membrane-derived oligosaccharide cycle) which is not present in eukaryotes and which therefore may be a target for novel antimicrobial agents. DAGK is also of interest as a system for studying membrane protein folding and stability and for studying membrane biocatalysis. Indeed, we and our collaborators (especially James Bowie of UCLA) have carried out extensive structure-function studies of DAGK which have led to assignment of specific roles for many residues in protein stability and catalytic function (Figure 1). The Bowie lab has also been attempting to grow high quality crystals of DAGK for about 7 years. While crystals can be grown, they diffract to only 11 angstroms.

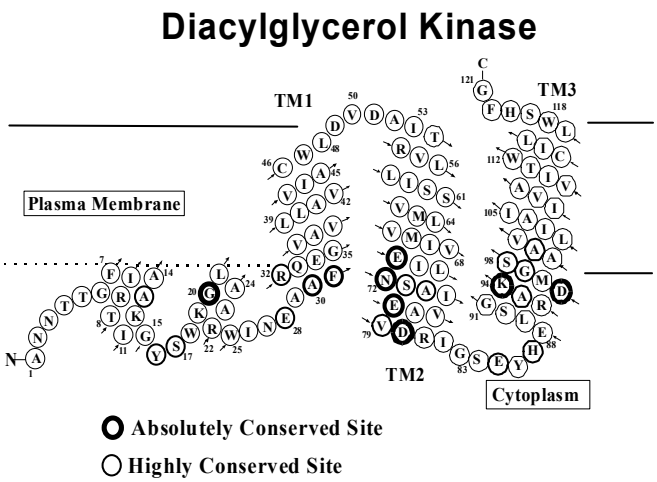

Figure 1. Topology of Diacylglycerol Kinase (DAGK) . DAGK functions as a homotrimer.

In collaboration with Dr. Sönnichsen, the Sanders lab has systematically optimized conditions under which high resolution NMR methods can be successfully applied to DAGK.

We now have reliable methods for producing triple-labeled DAGK and for preparing samples of this enzyme in detergent micelles, where the DAGK trimer/detergent aggregate mass is ca. 100 kDa. DAGK concentrations of 3 mM can be achieved and samples are completely stable for at least a week at 45°C.

EMSL has been quite generous by providing us with blocks of 800 MHz instrument time over the past year and prior to that. Based upon TROSY-based 3-D experiments conducted at EMSL using perdeuterated DAGK, we have completed assignment of about 80% of DAGK's 120 native backbone resonances (Figure 2). We have data which suggests that many of the remaining 20% of unassigned amide resonances are absent in the spectra because of a failure to completely back-exchange amide deuterons for protons following biosynthetic sample perdeuteration. We are now in the process of working out conditions for forcing such back-exchange so that the unassigned amide resonances can be viewed in otherwise fully perdeuterated samples. Moreover, we have also published a paper (Oxenoid 2002) which presents a preliminary description of DAGK's secondary structure based on analysis of the ^{15}N and ^{13}C NMR chemical shifts measured for assigned residues. The instrument time support of EMSL and assistance of Dr. Hoyt is acknowledged in that paper. It should also be noted Dr. Sanders acknowledged EMSL's support at the end of presentations on the DAGK NMR work at international conferences during the past year (Symposium session at the Biophysical Society Annual Meeting in San Francisco and Platform session at the ICMRBS meeting in Toronto).

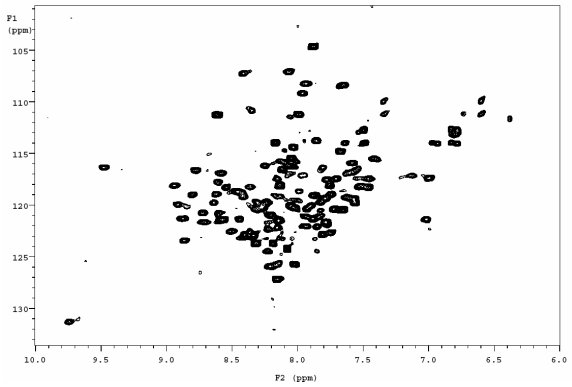

Figure 2. 800 MHz TROSY Spectrum of Triple Labeled DAGK in DPC Micelles at 45 degrees acquired at EMSL. 80% of DAGK's backbone amide resonances have now been assigned (Vinogradova et al. 1997b). (Downfield Trp indole NH peaks are not shown).

With assignments nearing completion, the shift of the DAGK NMR project is towards the acquisition of restraints for structural determination (NOEs and residual dipolar couplings). While the Sanders lab has moved to Vanderbilt, the collaboration between his lab and that of Dr. Sönnichsen continues. Also, while there is an in-house 800 MHz NMR at Vanderbilt we will continue to request time at the EMSL facility, particularly for 900 MHz time. Experiments to measure NOEs and dipolar couplings are likely to be extremely demanding because of the relatively wide line widths yielded by DAGK (even in TROSY spectra) and resulting sensitivity problems—such measurements should benefit significantly from access to 900 MHz instrumentation.

References

Ashish, A, F Abildgaard, JH Bushweller, and LK Tamm. Structure of outer membrane protein A transmembrane domain by NMR spectroscopy. *Nature Structural Biology*, **8**, 334-338 (2001).

Fernandez, C, K Adeishvili, and K Wuthrich. TROSY with the outer membrane protein OmpX in dihexanoyl phosphatidylcholine micelles. *Proc. Nat. Acad. Sci.*, **98***,* 2358-2363 (2001).

Hwang, PM, W Choy, EI Lo, L Chen, JD Formay-Kay, CRH Raetz, GG Prive, RE Bishop, and LE Kay. Solution structrure and dynamics of the outer membrane protein PagP by NMR. *Proc. Nat. Acad. Sci.*, **99***,* 13560-13565 (2002).

Kennedy, EP. Membrane-derived oligosaccharides of *E. coli.* In "*E. coli and S. typhimurium: Cellular and Molecular Biology.*" Vol. I, 2nd ed., pp. 1064-1071, F. C. Neidhardt, Ed., ASM Press, Washington (1996).

Lau, FW, X Chen, and JU Bowie. Active sites of *E. coli* DAGK are shared between subunits. *Biochemistry*, **38**, 5521-5527 (1999).

Nagy, JK, WL Lonzer, and CR Sanders. Kinetic study of Folding and misfolding of diacylglycerol kinase in model membranes. *Biochemistry*, **40***,* 8971-8980 (2001).

Oxenoid, K, FD Soennichsen, and CR Sanders. Conformationally-specific misfolding of an integral membrane protein. *Biochemistry*, **40***,* 5111-5118 (2001).

Oxenoid, K, FD Sonnichsen, and CR Sanders. Topology and secondary structure of the N-terminal domain of diacylglycerol kinase. *Biochemistry*, **41**, 12876-12882 (2002).

Sanders, CD and K Oxenoid. Customizing model membrane and samples for NMR spectroscopic studies of complex membrane proteins. *Biochimica et Biophysica Acta* **1508**, 129-145 (2000).

Vinogradova, O, F Sonnichsen, and CR Sanders. On Choosing a Detergent for Solution NMR Studies of Membrane Proteins. *J. Biomolecular NMR,* **4**, 381-386 (1997a).

Vinogradova, O, P Badola, L Czerski, F Sonnichsen, and CR Sanders. *E. Coli* diacylglycerol Kinase: A Case Study in the Application of Solution NMR Methods to An Integral Membrane Protein *Biophysical Journal* **72**, 2688-2701 (1997b).

Ultra-high Field NMR Study of Stable Isotope Applications

K McAteer,[(a)] GW Buchko,[(a)] NG Isern,[(a)] LA Silks,[(b)] R Michalczyk,[(b)] and MA Kennedy[(a)]

(a) Pacific Northwest National Laboratory

(b) Los Alamos National Laboratory

We are developing and implementing new approaches for using isotopic labels in NMR-based DNA structure determination. DNA structure determination by NMR spectroscopy is an under-restrained problem in general. We recently reported the results of an *in silico* experiment that show that the force fields used in restrained molecular dynamics calculations can be significant compared to the NMR restraints in driving the final structures to converge. Figure 1 shows the progressive improvement in the DNA structure in going from NOEs only to inclusion of all classes of restraints including residual dipolar couplings. Isotopic labeling considerably increases the number and type of NMR experiments than can be collected on DNA samples, thus increasing the potential number and classes of restraints that can be used in NMR-based DNA structure calculations. Consequently, the force field dependence can be potentially overcome resulting in significant improvements in both global and local structure of a DNA duplex. This has important implications when interpreting local fine structure, especially when investigating distortions to DNA resulting from DNA damage. To our knowledge, no NMR-based damaged DNA structures have been solved with the benefit of isotope labeling.

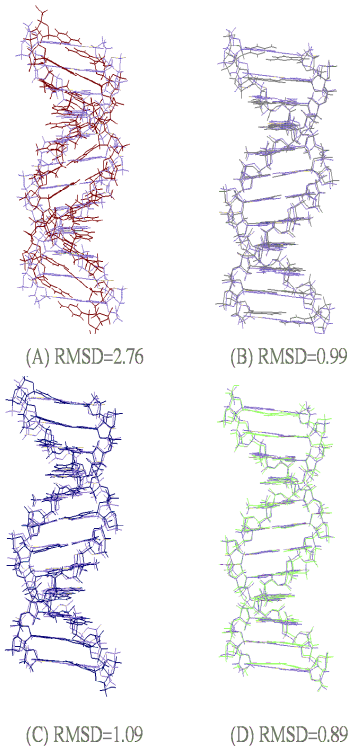

Figure 1. Lowest energy structures of the Dickerson dodecamer superimposed on B-DNA calculated with (A)NOE restraints (B) NOEs and one residual dipolar coupling per base (C) NOEs and dihedrals (D) NOEs and dihedrals and one residual dipolar coupling per base.

This year we have explored an alternative approach for measuring residual dipolar couplings in overlapped regions of spectra with ^{15}N-,^{13}C-labeled ubiquitin. We select any one of the four TROSY or anti-TROSY components of a 2-D coupled quartet in a ^{13}C-^{1}H CT-HSQC experiment, measure the frequency difference between the individual components, and from this measure the residual dipolar couplings. This approach provides us with a means of resolving overlapped cross-peaks and will be of particular interest in the crowded sugar regions of DNA spectra. We have collected ^{15}N-^{1}H HSQC and ^{13}C-^{1}H HSQC spectra on the following two specifically-labeled DNA oligomers that contain the biologically important TpA step (residues in bold contain ^{15}N and ^{13}C labels):

[d(CG**A**G**G**T**T**T**A**A**A**C**C**T**C**G)$_2$] [d(C**G**A**G**G**T**T**T**A**A**A**C**C**T**CG)$_2$]

Each oligomer was divided into two samples, one acting as a control and the second was aligned at 500 MHz in 25 mg mL^{-1} of Pf1 bacteriophage. Spectra are shown in Figure 2. We are using these data to refine the three-dimensional structure of the DNA duplex.

A significant part of this project is directed at producing isotopically labeled DNA samples. During this year we have also collected NMR data on the following ^{15}N-,^{13}C-labeled oligomers: 5'-GG**G**AA**C**A**C**T**A**G-3':5'-CC**C**T**T**G**T**T**G**A**T**C-3' and 5′-GG**G**AT**C**CA**C**TAG-3′:3′-CCC**T**AG**GT**GATC-5′ which contain 8-oxoguanine (underlined), a stable product of oxidative DNA damage. 8-Oxoguanine is a substrate for base excision repair (BER) by DNA glycosylases enzymes that recognise and remove damaged DNA bases. With these data we are studying the structure and dynamics of the damaged DNA in different sequence contexts to identify the properties at the damaged site that are responsible for recognition by the DNA glycosylases.

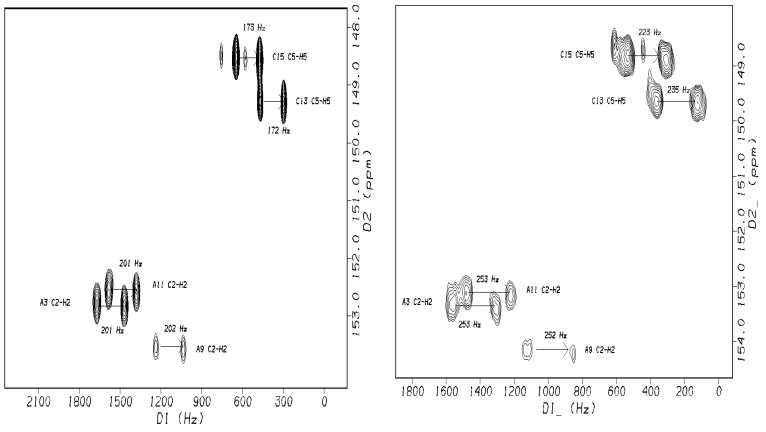

Figure 2. (A) ^{13}C-^{1}H couplings measured in the C2-H2 and C5-H5 region of a 500 MHz HSQC spectrum of the control sample [d(CG**A**G**GTTA**A**C**T**C**G)$_2$] and (B) ^{13}C-^{1}H couplings measured in the C2-H2 and C5-H5 region of a 500 MHz HSQC spectrum of [d(CG**A**G**GTTA**A**C**T**C**G)$_2$] dissolved in 25 mg mL^{-1} Pf1 bacteriophage solution.

We have also developed new methods for accurately determining the ^{1}H-^{1}H coupling constants in the sugar ring of DNA. Short transverse relaxation times coupled with high local proton densities in DNA leads to efficient dipolar relaxation and corresponding broad resonance lines. These broad lines together with spectral overlap and transverse cross-relaxation effects complicate the process of extracting meaningful coupling constants in DNA. Manuscripts describing the work have been published and the work will aid in the analysis of the structure and dynamics of the sequences described above.

References

McAteer, K, and MA Kennedy. Force Field Dependence of NMR-Based, Restrained Molecular Dynamics DNA Structure Calculations Including an Analysis of the Influence of Residual Dipolar Couplings. *J. Biomol. Struct. Dyn.* **20**, 487-506 (2003).

Yang, J, K McAteer, LA Silks, R Wu, NG Isern, CJ Unkefer, and MA Kennedy. A Comprehensive Approach for Accurate Measurement of Proton-Proton Coupling Constants in the Sugar Ring of DNA. *J. Mag. Reson.* **146**, 260-276 (2000).

Yang, J, LA Silks, R Wu, NG Isern, CJ Unkefer, and MA Kennedy. Improvements for Measuring Approach for 1H-1H Coupling Constants in DNA Via New Stripe-Cosy and Superstripe-Cosy Pulse Sequences Combined with a Novel Strategy of Selective Deuteration. *J. Mag. Reson.* **129**, 212-218 (1997).

Interaction of *Escherichia Coli* Formamidopyrimidine-DNA Glycosylase (Fpg) With DNA Containing an Abasic Site Analogue: Solution Studies Using NMR Spectroscopy

GW Buchko ,[(a)] K McAteer,[(a)] SS Wallace,[(b)] and MA Kennedy[(a)]

(a) Pacific Northwest National Laboratory

(b) University of Vermont, Burlington

Free radical mediated damage to DNA is believed to be the most important mechanism responsible for mutagenesis, carcinogenesis, aging, and various diseases. Exposure to ionizing radiation, near UV light, and chemical oxidants can generate free radicals. However, most free radicals are generated in normal cellular metabolic processes. To avoid mutations and cell death due to the accumulation of DNA damage, cells have developed several DNA repair strategies. Among these is the base excision repair (BER) pathway. In prokaryotes an important BER enzyme is formamido-pyrimidine-DNA glycosylase (Fpg). The principle biological role of Fpg is to remove the promutagenic DNA lesion 7,8-dihydro-8-oxoguanine (8-oxoG) although it also removes many other lesions *in vitro*. *Escherichia coli* Fpg is a 269 residue protein with a molecular weight of 30.2 kDa. Using extended X-ray fine structure spectroscopy, we have recently shown that Fpg contains a C4-type zinc-binding motif located at the C-terminal of the protein (Buchko et al. 2000). Fpg is a bifunctional DNA glycosylase/ β,δ-lyase that initiates damage removal via nucleophilic substitution at C1' by the N-terminal proline (P2). Using instrument time at the NMR facilities in the EMSL, we are conducting experiments designed to help us understand the details on how Fpg recognizes and removes 8-oxoG and other oxidized bases from genomic DNA. While the high molecular weight of Fpg (30.2 kDa) coupled with its low solubility (maximum ~ 0.8 mM) made backbone assignments difficult, substantial progress was made using a combination of residue specific labeling and perdeuteration of the protein (Buchko et al. 2001). With these assignments and an homology model for *E. coli* Fpg derived from the crystal structure of *T. thermophilus* Fpg (Figure 1), it was possible to study molecular dynamics at specific sites on the proteins surface using relaxation experiments. For these NMR studies a 13-residue 2x-DNA oligomer containing an abasic site analogue (1,3-propanediol) was used to probe changes to Fpg upon DNA binding. This DNA, 13-PD, forms a stable, non-covalent complex with Fpg (K_d ~ 2.9 nM). However, 13-PD itself is not a substrate for Fpg. A crystal structure of *L. lactis* Fpg non-covalently bound to 13-PD was recently solved (Serre et al. 2002). While a crystal structure provides valuable information, it is only a snapshot of the molecule in one state. Using NMR spectrometry it is possible to study molecular dynamics. Protein motion in the ms to μs time-scale may be followed using ^{15}N-^{1}H CPMG-HSQC

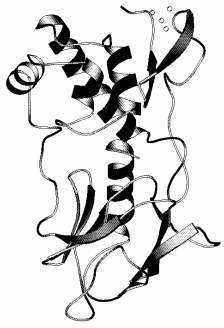

Figure 1. Homology model for *E.coli* Fpg generated using Swiss-Model and the crystal structure of *T. thermophilus* Fpg (Sugahara et al. 2000).

experiments. Such motion may play an important role in transient conformational rearrangements necessary to expose a binding pocket to its substrate or to lock a substrate in place for catalysis. Such experiments were performed on Fpg with and without DNA and are plotted in Figure 2. Slow motion observed for D91 and H92 are "frozen-out" with the addition of 13-PD. These residues are adjacent to residue H90 that makes a specific contact with 13-PD in the Fpg/13-PD crystal structure. One of the "mysteries" about Fpg's function is how it is able to recognize and repair many chemically distinct DNA base lesions. One theory is that all the base lesions recognized by Fpg perturb the phosphodiester backbone locally at the lesion site and it is this perturbation that Fpg recognizes. The ^{31}P chemical shifts of DNA are very sensitive to the conformation of the phosphodiester backbone. The ^{31}P resonances for the normal 13-mer, 13-GC, all lie within a narrow range around -4.2 ppm. The ^{31}P NMR spectrum of 13-PD shows two resonances at 15°C. These ^{31}P resonances have been assigned to the phosphates on both sides of 13-PD and suggest that the phosphodiester backbone is perturbed in 13-PD with the perturbation localized about the AP-site. On the addition of Fpg to excess 13-PD, the downfield ^{31}P resonances disappear. The *L. lactis* Fpg/13-PD crystal structure shows the DNA is double-helical when bound to Fpg, however, there is a 60º bend in the DNA at the AP-site (Serre et al. 2002). Such a bend should produce drastic changes in the ^{31}P resonances about the AP-site. It may be that the ^{31}P resonances of 13-PD around the AP-site become too broad to be observed upon binding to Fpg (30.2 kDa).

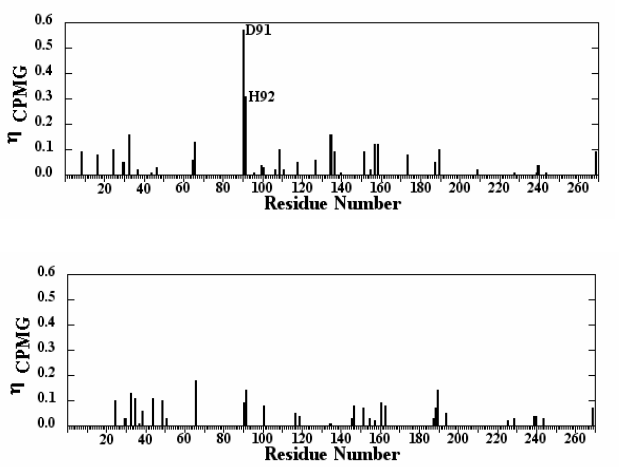

Figure 2. Enhancement factors (nCPMG) for Fpg alone (top) and upon the addition of excess 13-PD (bottom). Large changes are observed for D91 and H92.

References

Buchko, GW, NJ Hess, V Bandaru, SS Wallace, and MA Kennedy. Spectroscopic studies of zinc(II)- and cobalt(II)-associated *Escherichia coli* formamidopyrimidine-DNA glycosylase: Extended X-ray absorption fine structure evidence for a metal-binding domain. *Biochemistry*, **39**, 12441-12449 (2000).

Buchko, GW, SS Wallace, and MA Kennedy. Base excision repair: NMR backbone assignments of *Escherichia coli* formamidopyrimidine-DNA glycosylase. *Journal of Biomolecular NMR*, **22**, 301-302 (2001).

Serre, L, K Pereira de Jésus, S Boiteux, C Zelwer, and B Castaing. Crystal structure of the *Lactococcus lactis* formamidopyrimidine-DNA glycosylase bound to an abasic site analogue-containing DNA. *EMBO,* **21**, 2854-2865 (2002).

Sugahara, M, T Mikawa, T Kumasaka, M Yamamoto, R Kata, K Fukuyama, Y Inoue, and S Kuramitsu. Crystal structure of a repair enzyme of oxidatively damaged DNA, MutM, from an extreme thermophile, *T. thermophilus*. *EMBO J*., **19**, 3857-3869 (2000).

NMR Structure of Exchangeable Apolipoproteins

C Xu,[(a)] D Fan,[(a)] D Hoyt,[(b)] and J Wang[(a)]
(a) Southern Illinois University at Carbondale
(b) Pacific Northwest National Laboratory

Our research involves NMR structural studies of the important proteins involved in cholesterol/lipid metabolism/transport. Currently, we are focusing on several exchangeable apolipoproteins, including human apolipoprotein E (apoE), apolipoprotein A-I (apoA-I) and insect apolipophorin-III (apoLp-III). These proteins play key roles in lipoprotein transport via the LDL-receptor mediate endocytosis (apoE) and reverse cholesterol transport to clear "bad" cholesterol (apoAI and apoE). ApoE is a 299-residue protein and apoAI is a 243-residue protein. Both proteins undergo a concentration-dependent aggregation. We are interested in NMR structural studies of both lipid-free and lipid/lipoprotein-bound states. Due to the large size of these complexes, a high-field NMR instrument is critical for this project and Southern Illinois University does not have such an instrument.

During the past two years, we applied for high-field NMR user time at PNNL every six months. On average, we have received 1–2 weeks of 750/800 MHz NMR time every six months. Using these high-field NMR instruments, we have collected, either remotely or on-site, NMR data for all three proteins. We strongly believed that the data collected on high-field NMR instruments significantly improved the NMR spectra of these larger proteins, making the NMR assignment possible. Figure 1 shows ^{15}N-edited NOESY spectra of apoLp-III/DPC micelles complexes collected on a 800 MHz (Panel A) using a triple-labeled sample and on a 500 MHz using a double-labeled sample (Panel B). It can be clearly seen that the spectral quality is significantly improved. The apoLp-III/DPC micelles have a molecular weight of ~42 KDa. With the high quality spectra collected on high field instrument, we are able to start to carry out a complete NMR assignment of this apoLp-III/DPC complex. Another example is our apoAI project. Figure 2 once again shows ^{15}N-edited NOESY spectra of apoAI(1-186) sample collected on a 750 MHz (Panel B) using a triple-labeled sample and on a 500 MHz using a double-labeled sample (Panel A). ApoAI(1-186) is a 24 kDa protein which is in the edge of requiring a triple-labeled sample.

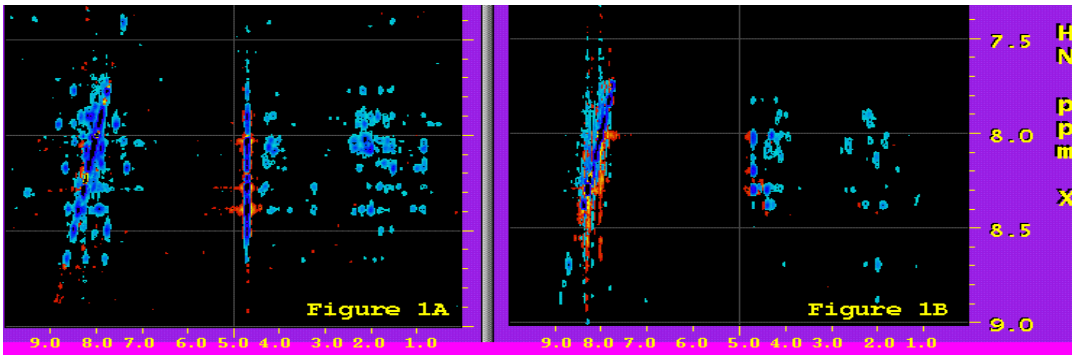

Figure 1. Panel A: Plane 31 of ^{15}N-edited NOESY-TROSY spectrum of a triple 60%2H, ^{13}C/^{15}N-labeled apoLp-III/DPC complex, @pH6.4, 30°C at 750 MHz (N=118.89 ppm). Panel B: Plane 31 of ^{15}N-edited NOESY spectrum of a double ^{13}C/^{15}N-labeled apoLp-III/DPC complex, @pH6.4, 30°C at 500 MHz (N=118.89 ppm).

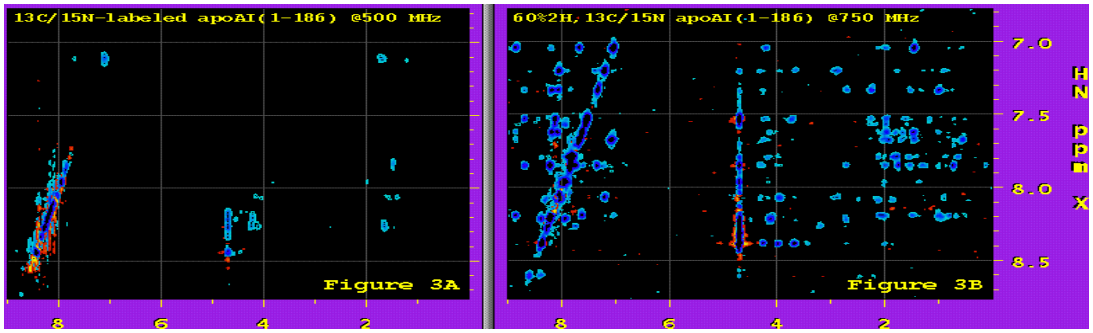

Figure 2. Panel A: ^{15}N-edited NOESY spectra of ApoAI(1-186) sample collected on a 500 MHz using a double-labeled sample. Panel B: Collected on a 750 MHz using a triple-labeled sample.

Indeed, a triple-labeled apoAI(1-186) at a high-field really dramatically improved the spectra quality. We were very happy once we saw this critical spectral improvement, however, we have recently found that apoAI(1-186), like full-length apoAI, aggregates in a concentration-dependent manner. At a lower concentration, such as 5 mg/ml (we measured τc using ^{15}N-T1/T2 at this concentration), apoAI(1-186) is > 90% monomeric. This result is confirmed by cross-linking experiment. At a higher concentration, such as 20–25 mg/ml, which is our sample concentration for 3D experiments, apoAI(1-186) is about 60% monomer and 35% dimer and 5% trimer and tetramer. We are currently working on sample conditions and preparing series mutants in order to search for a condition in which apoAI(1-186) is monomeric. We have mutated three large hydrophobic residues by an Ala or Asn, and found this mutant is ~90% monomeric with only 10% dimer at 20mg/ml. We have collected preliminary NMR data on our 500 MHz instrument, and will collect 3-D 15N-edited NOESY on a high-field instrument at PNNL soon.

The data we collected on high-field instruments at PNNL significantly improved the spectral quality of several large protein or protein/lipid system. This improvement makes our project possible to continue. Based on these preliminary results, we have applied for several grants, including two NIH RO1 applications. We have received an International HDL Research Award for our apoAI(1-186) project. This is an important achievement for the Southern Illinois University laboratory since only 12 applications were funded worldwide and our application is one of these 12 funded proposals. We truly believe that we would not be able to receive this funding if we did not have our preliminary high-quality NMR spectra collected at PNNL.

We are very happy with the service provided by PNNL. The staff there are always very helpful, especially David Hoyt and Joe Ford. They usually help us to set up experiments till late in the evening. This is extremely helpful since most of the time, we were using PNNL remotely. We are > 1,000 miles away from PNNL, a remote operation could be a problem. However, with the help from the PNNL staff, our operations always went very smoothly.

References

Fan, D, LR Reese, PM Weers, RO Ryan, and J Wang. A complete assignment of an exchangeable apolipoprotein – L. migratoria apolipophorin-III. *J. Biomol-NMR.* **19**, 83-84 (2001).

Fan D, LA Reese, Q Li, and J Wang. NMR structure of an exchangeable apolipoprotein – L. migratoria apoLp-III (in press).

Solid-State NMR Spectroscopy of Quadrupolar Nuclei at High Magnetic Field Strengths

DL Bryce,[(a)] KW Feindel,[(a)] MA M Forgeron,[(a)] M Gee,[(a)] KJ Ooms,[(a)] and RE Wasylishen[(a)]
(a) University of Alberta, Canada

During the past two years, we have made four trips to the Pacific Northwest National Laboratory (PNNL) to use the high magnetic field nuclear magnetic resonance (NMR) spectrometers and have received 24 days of NMR time on either the 17.6 or 18.8 T NMR systems. The NMR properties and low natural abundance of most of the nuclei that we have investigated (^{25}Mg, $^{35/37}$Cl, ^{53}Cr, ^{91}Zr, and ^{95}Mo) render them difficult to observe via NMR spectroscopy. The use of high applied magnetic field, B_0, strengths is critical as it facilitates measurement of the chemical shift (CS) tensor and reduces the line width of the central transition arising from the second-order quadrupolar interaction.

The all-encompassing goal of our research is to explore the potential of NMR spectroscopy in characterizing solid materials. We are particularly interested in examining "traditionally difficult" quadrupolar nuclei that are important in materials science and structural biology. NMR investigations of quadrupolar nuclei are capable of providing subtle information about the orientation dependence of the CS and electric field gradient (EFG) at a particular nuclear site. We hope that our exploratory research will demonstrate the feasibility and potential of solid-state NMR spectroscopy involving quadrupolar nuclei with small magnetic moments.

This report includes a summary of our ^{53}Cr and ^{95}Mo NMR results. Additional studies, not shown here, were performed on ^{11}B, ^{25}Mg, $^{35/37}$Cl, and ^{91}Zr.

***^{53}Cr and ^{95}Mo Solid-State NMR Spectroscopy*:** During our last three visits at PNNL, we have succeeded in obtaining high-field ^{95}Mo NMR spectra of several molybdate salts and mesitylenetricarbonylmolybdenum(0), as well as ^{53}Cr NMR spectra of a series of solid chromate salts and one dichromate salt. The ^{95}Mo NMR work on mesitylenetricarbonyl-molybdenum(0) is summarized in a full manuscript (Bryce and Wasylishen 2002).

The object of the work on the MO_4^{2-} (M = Cr, Mo) series of compounds is to characterize the CS and EFG interactions at the metal nuclei and to determine their relationship to structure. Earlier research indicates that, while the CS tensors are sensitive to the local environment and symmetry, the EFGs depend on both local and long-range symmetry. Our initial studies on solid $Cr(CO)_6$ and $Mo(CO)_6$ suggest a remarkable correspondence in the Cr and Mo CS tensors. Similarities between the NMR parameters of the series of CrO_4^{2-} and MoO_4^{2-} compounds will be investigated.

Use of the quadrupolar Carr-Purcell-Meiboom-Gill (QCPMG) pulse sequence was of paramount importance in the study of both the chromate and molybdate salts, providing high-quality spectra with excellent signal-to-noise. Our ^{53}Cr QCPMG NMR spectra of the chromates, examples of the first reported chromium NMR studies of diamagnetic solids,

were presented at *The Canadian Society for Chemistry* conference held in Vancouver, BC in June, 2002. Preliminary results for the ^{53}Cr CS and quadrupole parameters were obtained. As well, correlations between the magnitude of $C_Q(^{53}Cr)$ of various chromate salts and the average deviation of the O-Cr-O angle from perfect tetrahedral symmetry (*i.e.*, 109.47°) were found and were rationalized in terms of the increased EFG at the chromium nucleus. The ^{53}Cr NMR spectrum of solid K_2CrO_4 acquired at 18.8 T using the QCPMG pulse sequence is shown in Figure 1. Relativistic DFT calculations of the magnetic shielding and EFG tensors were also carried out on the chromate salts. Qualitative agreement between experimental and theoretical results was found.

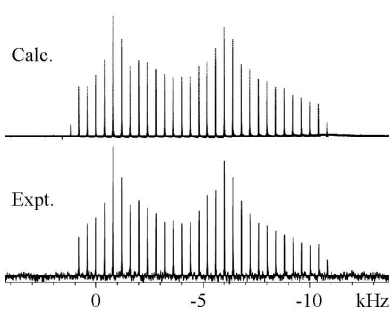

Figure 1. Calc. (top) and Expt. (bottom) ^{53}Cr QCPMG NMR spectra of solid K_2CrO_4.

In October 2002, ^{95}Mo QCPMG NMR spectra of several molybdenum salts were obtained and are currently being analyzed to extract the ^{95}Mo CS and EFG parameters. The ^{95}Mo QCPMG NMR spectrum of $MgMoO_4$ is shown in Figure 2. The analysis of the ^{53}Cr and ^{95}Mo solid-state NMR spectra of the chromate and molybdate salts is being facilitated using spectra acquired on our 11.75 T spectrometer. Further high-field solid-state NMR experiments will be carried out at PNNL in March, 2003 on an extended series of chromate and molybdate salts. Our long-range goal is to examine the potential of solid-state NMR in characterizing early transition metal polyoxometalates. Access to the NMR facilities at PNNL has demonstrated the importance of working at the highest possible magnetic field strengths.

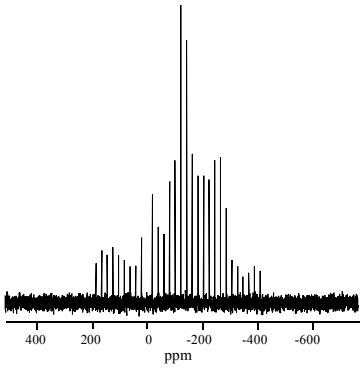

Figure 2. ^{95}Mo QCPMG NMR spectrum of $MgMoO_4$ ($\mathbf{B_0}$ = 17.6 T).

References

Bryce, DL and R E Wasylishen. *Phys. Chem. Chem. Phys.*, **4**, 3591 (2002).

Bryce, DL and RE Wasylishen. *Phys. Chem. Chem. Phys.*, **3**, 5154 (2001).

Eichele, K, RE Wasylishen, and JH Nelson. *J. Phys. Chem. A*, **101**, 5463 (1997).

Larsen, FH, AS Lipton, HJ Jakobsen, NChr Nielsen, and PD Ellis. *J. Am. Chem. Soc.*, **121**, 3783 (1999).

Polyoxometalate Chemistry: From Topology via Self-Assembly to Applications, edited by MT Pope and A Müller, Kluwer Academic (2001).

Polyoxometalate Chemistry for Nano-Composite Design, edited by T Yamase and MT Pope, Kluwer Academic (2001).

Smith, ME. *Annu. Rep. NMR. Spectrosc.*, **43**, 121 (2001).

Spatial Properties of Trapped Free Radicals in Irradiated DNA Model Systems at Low Temperatures

MK Bowman[(a)] and JD Zimbrick[(b)]
(a) Pacific Northwest National Laboratory
(b) Purdue University, West Lafayette, Indiana

Ionizing radiation deposits its energy inhomogeneously in living cells. In DNA this pattern of deposition results in multiple damaged sites (MDS) consisting of one or more free radicals localized in a microscopic volume on the order of several tens of nanometers in diameter. These localized free radicals react to form stable sugar and base damage products. The complexity of damage in these sites and their spatial density is thought to vary with the energy and type of radiation being used, e.g., x-rays that produce the least complex sites versus heavy ions such as alpha particles, that produce much more complex sites. Further, it is thought that increases in complexity and spatial density of damage in these sites correlate with observed increasing biological effects for these various kinds of radiations. A major challenge in molecular radiobiology is to obtain accurate experimental information about these properties of MDS. In this project we are attempting to obtain experimental measurements of the spatial characteristics of free radicals in MDS as well as the distribution of stable damage products resulting from the radical reactions produced in DNA after it has been irradiated with radiations of various types and energies. Experimental values of these parameters are important as inputs to models of radiation damage to the genome from low doses of radiation. The expectation is that these models may be useful in predicting the health effects of low doses of ionizing radiation. The distributions of stable damage products are being determined at Purdue University by use of high-performance liquid chromatography (HPLC) and mass spectrometric methodologies.

The spatial parameters of MDS are being studied by use of pulsed electron paramagnetic resonance (EPR) measurements. The EPR theory that can be used to calculate spatial parameters of trapped free radicals in solids has been developed (Maryasov et al. 1998; Milov et al. 1998), but has not heretofore been applied to biological radicals trapped in MDS in DNA. It involves a technique called pulsed electron-electron double resonance (PELDOR) to examine dipolar interactions between radicals trapped in the MDS at low temperatures. PELDOR data, combined with appropriate theory, can yield values of average spacing between radicals and average local concentrations of radicals as well as average MDS dimensions for various types of radiations. We are using our allotted EPR time at EMSL to adapt the PELDOR theory to MDS and to make PELDOR measurements on a set of DNA samples irradiated with heavy (^{36}Ar) ions. We use a PELDOR refocused echo detection technique introduced by Jeschke et al. (2000) and shown in Figure 1. An electron spin echo signal is generated by a series of three microwave pulses, all at the observing frequency, shown in the figure as solid blocks. The first two pulses, separated by a time known as τ, produce a two-pulse primary echo following the second pulse by a delay of τ. The third pulse at the "solid" observing frequency regenerates or refocuses the spin echo which is then measured. During the generation of the refocused echo, an additional microwave pulse at a second 'pumping' frequency is applied. The PELDOR time-domain spectrum is the record of the refocused echo intensity as a function of the position of the pumping pulse between the second and third observation pulses. If the pumping pulse is applied simultaneously

with the primary echo, there is no effect on the intensity of the refocused echo, but if there is a delay between the pumping pulse and primary echo, any interaction between the set of pumped free radicals and the set of detected free radicals will result in a decrease in the detected refocused echo intensity. The stronger those interactions, the shorter the delay at which an intensity decrease will become apparent. In most samples containing simple free radicals, the interactions between free radicals is magnetic dipolar in nature and varies with the inter-radical distance, r, as $1/r^3$. Thus the PELDOR signals are quite sensitive to the spatial distribution functions of free radicals and can be used as a means of quantitatively measuring the number and distribution of the closer neighbors.

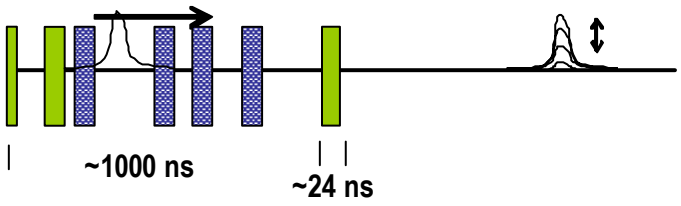

Figure 1. Refocused Echo method for measuring distances between free radicals in irradiated DNA. Solid bars represent microwave pulses at one frequency that generate the detected echo signal at right. The hatched bars represent one pulse of a different microwave frequency whose position in time is swept during the measurement.

Two typical PELDOR spectra obtained from a DNA sample irradiated with a ^{36}Ar dose of 15kGy were collected. Such spectra are obtained for various pumping pulses that result in differing fractions of radicals being affected by the pulse. The spectra all show a monotonic, roughly exponential decay of the signal with rates that increase with increasing fractions of affected radicals and with a non-zero asymptote at long decay times. The observation that the PELDOR decays are roughly exponential with non-zero asymptotes can be interpreted by use of the theoretical and experimental work of Tsvetkov et al. This interpretation requires that the spatial distribution of the neighboring radicals in an MDS be uniform or nearly uniform and yields an estimate of about twenty radicals contained therein. These MDS can be visualized as corresponding to short segments of individual ^{36}Ar ion tracks. Further analysis for the average MDS yields an approximate radius of about 7 nm.

We are proposing to continue these studies on DNA samples irradiated with various doses of radiations that differ in their amounts of energy deposited per unit track length. The results should provide new information about the spatial properties of the radicals that will help to characterize MDS in ways not previously possible.

References

Maryasov, AG, YD Tsvetkoc, and J Raap. Weakly coupled radical pairs in solids: ELDOR in ESE structure studies. *Applied Magnetic Resonance,* **14**(1), 101-113 (1998).

Milov, A, AG Maryasov, and YD Tsvetkov. Pulsed Electron Double Resonance (PELDOR) and Its Applications in Free Radicals Research. *Applied Magnetic Resonance,* **15**, 107-143 (1998).

Pannier, M, S Viet, A Godt, G Jeschke, and HW Spiess. Dead-Time Free Measurement of Dipole-Dipole Interactions Between Electron Spins. *Journal of Magnetic Resonance,* **142**, 331-340 (2000).

User Projects

Structural Characterization of p53,c-Myc and the Protein-Protein Interactions that Regulate Their Biological Activity

Structural Proteomics: Annotating the genome Using 3D Structure

Dissecting Apoptotic and Growth Regulatory Pathways Using Structural Biology
CH Arrowsmith
University of Toronto, Canada

Structural Characterization of a Dynein Light Chain Homodimer

Structure and Interactions of 25 kDa Dynein Light Chain Homodimer
E Barbar,
Ohio University, Athens

Biofilm Studies Using Multi-Modal Molecular Imaging Agents
DJ Bornhop
Texas Tech University, Lubbock
FJ Brockman
Pacific Northwest National Laboratory

EPR Study of Paramagnetic Centers in Gamma-Irradiated Polycrystalline Ammonium Nitrate
AP Bussandri
Quantum Magnetics, San Diego, California

^{11}B MAS NMR Spectroscopy of Amorphous Metal Boride Hydrotreating Catalysts
ME Bussell, J King, G Parks, ML Pease, S Sawhill
Western Washington University, Bellingham

Solution Al-27 NMR at 750 MHz (H1) of Methylaluminoxanes
LG Butler, JL Eilertsen, WD Treleaven
Louisiana State University, Baton Rouge

Structure Determination of the SWI1 DNA-Binding Domain

Application for NMR Time on the 800 MHz NMR Spectrometers to Characterize Substrate Recognition in the SUMO Pathway

Application for 800 MHz NMR Time for Structure Determination of the Ku80 C-Terminal Domain
Y Chen
Beckman Research Institute of the City of Hope, Duarte, California

The Evolution of Protein Flexibility
GW Daughdrill, K Kodali
University of Idaho, Moscow

Spectroscopic Analysis of Organic Compounds in Atmospheric Aerosols
S Decesari
Institute for Atmospheric and Oceanic Sciences, Bologna, Italy
LA Barrie
Pacific Northwest National Laboratory

High-Field NMR Studies of Very Large RNA Molecules: The VS Ribozyme
T Dieckmann, JC Flinders
University of California at Davis

Conformational and Dynamics Studies of Human Salivary Histatin Bound on Hydroxyapatite by Solid State NMR
GP Drobny, M Cotten
University of Washington, Seattle

Protein Design, Protein Recognition and Molecular Chaperones

Solution Structure of BAG Domains:BAG1 dN

BAG1 as a Link between Cell Growth and the Stress Response: An NMR Study

Structure of a Helical Signaling Domain from p130 Cas

Structure of a Helical Signaling Domain from Cas

Understanding Hepatitis B Infection Structure of Hepatitis B Virus x Protein Bound to its Cellular
KR Ely, K Briknarova
The Burnham Institute, La Jolla, California

NMR Structure Determination of EPSP Synthase Part IV
JN Evans, G Helms, JK Young
Washington State University, Pullman

Separating the Lineshapes of the Two NMR Active Ti Isotopes by Static QCPMG solid-state NMR experiments
I Farnan
University of Cambridge, United Kingdom
FH Larsen
University of Copenhagen, Denmark

Visualization of Colloid Transport in Hanford Sediments

Solid State NMR of ^{133}Cs Incorporated into and Adsorbed onColloids formed in Soils Reacted with Hanford Tank Waste Solutions
M Flury
Washington State University, Pullman

Technique Development, Further Studies of Ultra-stable Acid Zeolites, Investigations of AIP04 Materials, Studies of Ceramic Materials

Further Studies of Ultra-Sable Acid Zeolites; Investigations of AIPO4 Materials; Studies of Ceramic Materials; Spin 1/2 Nuclei
C Fyfe, JL Bretherton, D Brouwer, AR Lewis
University of British Columbia, Canada

Very HF (Static) Broadline NMR Detection of Quadrupolar Nuclei

Solid State NMR Characterization of Synroc and its Constituent Phases

Solid-State NMR Characterization of Metal Phosphines

Solid-State NMR Characterization of Synroc
JV Hanna
ANSTO NMR Facility, Sydney, Australia

Solid State NMR of ^{133}Cs Incorporated into and Adsorbed on Colloids Formed in Soils Reacted with Hanford Tank Waste Solutions
JB Harsh, Y Deng
Washington State University, Pullman

Atomic-Level Structure of Silicon and Aluminum in Natural and Synthetic Minerals
NW Hinman
University of Montana, Missoula, Montana

NMR Structure of Sec35p/Cog2p
FM Hughson, L Cavanaugh, I Pelczer
Princeton University, Princeton, New Jersey

Mechanisms of Phosphorus Stabilization in the Soil Environment: A Molecular Scale Evaluation
S Hunger
University of Delaware, Newark

Develop probe for 21.15T Narrow Bore Magnet
HJ Jakobsen
Aarhus University, Denmark

Probing the Mechanism of the Alkaline Phosphatase Reaction by ^{67}Zn and ^{25}Mg NMR
ER Kantrowitz
Boston College, Chestnut Hill, Massachusetts

NMR Structural Investigations of BRCA1
RE Klevit, PS Brzovic
University of Washington, Seattle

Molecular Probes of Quinol Oxidation by the Cytochrome b6f Complex
DM Kramer, AG Roberts
Washington State University, Pullman

Multinuclear MAS NMR of Cesium Alumino-silicate Compounds
MJ Lambregts
Argonne National Laboratory West, Idaho Falls, Idaho

Characterization of Aquatic Organic Matter using NMR Spectroscopy
CK Larive, C Hellriegel
University of Kansas, Lawrence
CS Uyguner
Bogazici University, Bebek, Istanbul

Pulsed EPR Studies of Vanadium Catalysts

Pulsed EPR Studies of Transition Metal-Exchanged Zeolites and Molecular Sieves
SC Larsen, JF Woodworth
University of Iowa, Iowa City

Analysis of High Surface Area Aluminas by ^{1}H and ^{27}Al NMR Methods

Aluminum Coordination Environments in Alumina Abstract
DA Lindquist, GG Burnside
University of Arkansas Little Rock

Endor of Trityl Radicals
C Mailer
University of Chicago, Illinois

Nuclear Spin Relaxation Measurements for Structural Genomics

Structural Genomics of Eukaryotic Model Organisms
GT Montelione, RK Paranji
Rutgers University, Camden, New Jersey

High-Field Solid-State NMR Studies of Weathered Specimen Kaolinite Clays
KT Mueller, GS Crosson
Pennsylvania State University, State College

Solid-State 67Zn NMR of Synthetic Metalloprotein Models
G Parkin
Columbia University, New York City, New York

Solid-State Germanium-73 NMR Spectroscopy at High Magnetic Fields
G Penner
University of Guelph, Ontario, Canada

High-Field NMR Studies of Thyroid Tumor-Marker (Recombinant) Chromogranin A, Catecholamine/Ca^{2+}ATP Storage Complexes and its Bioactive Proteolytic Products
NE Preece
Burnham Institute, University of California San Diego
DT O'Connor
University of California San Diego

CP/MAS of -HMX at 18.8 Tesla
RJ Pugmire, JS Clawson
University of Utah, Salt Lake City

Solid State ^{113}Cd and ^{67}Zn NMR of Pyrazolyl-Borates and Methanes
DL Reger
University of South Carolina, Columbia

Activation of the Arp2/3 Complex by WASP Family Proteins: Probing Individual Subunits by NMR
MK Rosen, M Kreishman-Deitrick
University of Texas, Austin

Evaluation of Materials for Single-Spin Magnetic Resonance Force Microscopy
D Rugar
IBM Research Division, Westchester County, New York

Virtual Lung Validation Using Hyperpolarized ^{3}He MRI
BT Saam, R Jacob, G Laicher
University of Utah. Salt Lake City

Structural Determination of a Complex Membrane Protein, Diacylglycerol Kinase
CR Sanders
Vanderbilt University School of Medicine, Nashville, Tennessee
K Oxenoid
Case Western Reserve University, Cleveland, Ohio

Free Radical Processes in G-and Heavy Ion Irradiated DNA
MD Sevilla, D Becker
Oakland University, Rochester, Michigan

NMR Structure Characterization of Isotopically Labeled DNA Oligonucleotides

Ultra-High Field NMR Studies of Stable Isotope Applications
LA Silks III
Los Alamos National Laboratory

Structural Determination of a Complex Membrane Protein, Diacylglycerol Kinase
FD Sonnichsen
Case Western Reserve University, Cleveland, Ohio

NMR Studies of the Initial Reaction Products of Diacetylbenzene Isomers with Lysine and Proteins
PS Spencer
Center for Research on Occupational and Environmental Toxicology, Portland, Oregon
M Kim, MI Sabari
Oregon Health and Science University, Portland, Oregon

Structure of Allochromatium Vinosum DsrC Protein

Structural Proteomics of Myobacterium Tuberculosis
TC Terwillger
Los Alamos National Laboratory

Interaction of *Escherichia Coli* Formamidopyrimidine-DNA Glycosylase (Fpg) with Damaged DNA Containing an 7,8-Dihydro-8-Oxoguanine Lesion.

NMR-Based Solution Structure of *Escherichia Coli* Base Excision Repair Protein Formamidopyrimidine-DNA Glycosylase

Interaction of Formamidopyrimidine-DNA Glycosylase (Fpg) with Damaged DNA: Backbone Assignments, Chemical Shift Mapping, and Relaxation Studies.
SA Wallace
University of Vermont, Burlington

NMR Studies of Human Apolipoprotein-AI

NMR Studies of Human Apolipoprotein-E N-Terminal Domain

Structural Determination of the Lipid-Bound Conformation of ApoLp-III

Structural Determination of ApoLp-III/HDL Particles
J Wang, X Ren, C Xu
Southern Illinois University at Carbondale

Structural Biology of the DNA Repair Proteins: The Nudix Protein Family from the Extremely Radiation-Resistant Bacterium *Deinococcus Radiodurans*
DE Wemmer, S Holbrook
University of California at Berkeley

Use of NMR Microscopy to Examine the Sub-Pore-Scale Structure of Porous Media with Multiple Liquid/Solid Phases

Use of NMR Microscopy to Examine Biofilm Structure in Porous Media under Conditions of Fluid Flow

NMR Microscopy for Measurement of the Biomass Distribution within a Porous Media System
BD Wood
Oregon State University, Corvallis

Characterization of the Mineral Phases of Matrix Vesicles During Induction of Crystalline Mineral Formation
RE Wuthier
University of South Carolina, Columbia

An Extended Study of Solid Prototypal Chromium and Molybdenum Compounds Using ^{53}Cr and ^{95}Mo Nuclear Magnetic Resonance Spectroscopy

Solid-State NMR Spectroscopy of Half-Integer Spin Quadrupolar Nuclei at High Magnetic Field Strengths: A Continuing Study of Model Boron and Molybdenum Compounds

Solid-State NMR Spectroscopy of Half-Integer Spin Quadrupolar Nuclei at High Magnetic Field Strengths: A Continuing Study of Hydrochloride Salts and Zirconium Phosphates

Zr-91 Nuclear Magnetic Resonance Studies of Solid Zirconium Compounds

^{53}Cr Nuclear Magnetic Resonance Studies of Solid Prototypal Chromium Compounds

High-Field Solid-State NMR Spectroscopy of ^{99}Ru in Inorganic and Organometallic Ruthenium Compounds

High-Field Solid-State ^{25}Mg NMR Studies of Inorganic and Biological Magnesium Compounds
RE Wasylishen, KW Feindel, M Forgeron, KJ Ooms
University of Alberta, Canada
DL Bryce
Dalhousie University, Halifax, Nova Scotia

Spatial Properties of Clustered Free Radicals Produced in DNA and Biodosimeters by Ionizing Radiation
JD Zimbrick
Purdue University, West Lafayette, Indiana

Al-27 NMR Analysis of Lactate Media Containing Al Colloids
JE Amonette
Pacific Northwest National Laboratory

Develop Probe for 21.15T Narrow Bore Magnet
PD Ellis
Pacific Northwest National Laboratory

NMR Analysis for Sorbitol and Glutamic Acid Derivatives

NMR Analysis of Pyrrolidinone Precursors and Derivatives
JE Holladay
Pacific Northwest National Laboratory

Characterization of Structure of Polyvinylferrocene by NMR
L Liang
Pacific Northwest National Laboratory

The Evolution of Protein Flexibility
DF Lowry
Pacific Northwest National Laboratory

Use of NMR Microscopy to Examine Biofilm Structure in Porous Media under Conditions of Fluid Flow
PD Majors
Pacific Northwest National Laboratory

Use of NMR Microscopy to Examine Biofilm Structure in Porous Media under Conditions of Fluid Flow
KR Minard
Pacific Northwest National Laboratory

NMR Studies on Nano-Materials

Probing Mechanisms of Novel Templated Synthesis
L Wang
Pacific Northwest National Laboratory

Post Mortem Energy Metabolism and Water Characteristics in Rabbit m. Longissimus Studied by Dynamic Slow Speed MAS NMR Spectroscopy and Relaxometry
RA Wind
Pacific Northwest National Laboratory

Staff

David W. Hoyt, Technical Group Leader
(509) 373-9825, david.w.hoyt@pnl.gov

Sarah D. Burton, Senior Research Scientist
(509) 376-1264, sarah.burton@pnl.gov

Joseph J. Ford, Senior Research Scientist
(509) 376-2446, joseph.ford@pnl.gov

Donald N. Rommereim, Senior Research Scientist
(509) 376-2671, don.rommereim@pnl.gov

Nancy G. Isern, Science & Engineering Associate
(509) 376-1616, nancy.isern@pnl.gov

Jesse A. Sears, Science & Engineering Associate
(509) 376-7808, jesse.sears@pnl.gov

Matrixed Research Staff

David W. Koppenaal, Associate Division Director & Laboratory Fellow
(509) 376-0368, david.koppenaal@pnl.gov

Paul D. Ellis, Laboratory Fellow
(509) 372-3888, paul.ellis@pnl.gov

Robert A. Wind, Laboratory Fellow
(509) 376-1115, robert.wind@pnl.gov

Michael K. Bowman, Staff Scientist
(509) 376-3299, michael.bowman@pnl.gov

Michael A. Kennedy, Staff Scientist
(509) 372-2168, makennedy@pnl.gov
Senior Research Scientists

Garry W. Buchko, Senior Research Scientist
(509) 373-9826, garry.buchko@pnl.gov

Herman M. Cho, Senior Research Scientist
(509) 376-2685, hm.cho@pnl.gov

John R. Cort, Senior Research Scientist
(509) 376-4559, John.Cort@pnl.gov

Andrew S. Lipton, Senior Research Scientist
(509) 376-6633, as.lipton@pnl.gov

David F. Lowry, Senior Research Scientist
(509) 373-0755, david.lowry@pnl.gov

Paul Majors, Senior Research Scientist
(509) 376-0836, Paul.Majors@pnl.gov

Kevin Minard, Senior Research Scientist
(509) 373-9847, kevin.minard@pnl.gov